HHS Public Access

Author manuscript

Sci Transl Med. Author manuscript; available in PMC 2022 May 26.

Published in final edited form as:

Sci Transl Med. 2021 May 26; 13(595): . doi:10.1126/scitranslmed.abd7702.

Transient receptor potential canonical 5 mediates inflammatory mechanical and spontaneous pain in mice

Katelyn E. Sadler[1,†], **Francie Moehring**[1,†], **Stephanie I. Shiers**[2], **Lauren J. Laskowski**[1], **Alexander R. Mikesell**[1], **Zakary R. Plautz**[1], **Allison N. Brezinski**[1], **Christina M. Mecca**[3], **Gregory Dussor**[2], **Theodore J. Price**[2], **John D. McCorvy**[1], **Cheryl L. Stucky**[1,*]

[1]Department of Cell Biology, Neurobiology and Anatomy, Medical College of Wisconsin, Milwaukee, WI 53226, USA.

[2]School of Behavioral and Brain Sciences and Center for Advanced Pain Studies, University of Texas at Dallas, Richardson, TX 75080, USA.

[3]Department of Anesthesiology, Medical College of Wisconsin, Milwaukee, WI 53226, USA.

Abstract

Tactile and spontaneous pains are poorly managed symptoms of inflammatory and neuropathic injury. Here, we found that transient receptor potential canonical 5 (TRPC5) is a chief contributor to both of these sensations in multiple rodent pain models. Use of TRPC5 knockout mice and inhibitors revealed that TRPC5 selectively contributes to the mechanical hypersensitivity associated with CFA injection, skin incision, chemotherapy induced peripheral neuropathy, sickle cell disease, and migraine, all of which were characterized by elevated concentrations of lysophosphatidylcholine (LPC). Accordingly, exogenous application of LPC induced TRPC5-dependent behavioral mechanical allodynia, neuronal mechanical hypersensitivity, and spontaneous pain in naïve mice. Lastly, we found that 75% of human sensory neurons express *TRPC5*, the activity of which is directly modulated by LPC. On the basis of these results, TRPC5 inhibitors might effectively treat spontaneous and tactile pain in conditions characterized by elevated LPC.

*Corresponding author: cstucky@mcw.edu.
†These authors contributed equally to this work.

Author contributions:

K.E.S. planned, performed, and analyzed behavioral and electrophysiology experiments as well as wrote and edited the manuscript. F.M. planned, performed, and analyzed behavioral and electrophysiology experiments and edited the manuscript. S.I.S. planned, performed, and analyzed RNAscope experiments as well as wrote and edited the manuscript. L.J.L. planned, performed, and analyzed in vitro experiments; generated the TRPC5 stable cell lines; and edited the manuscript. A.R.M. planned, performed, and analyzed behavioral experiments and edited the manuscript. Z.R.P. planned, performed, and analyzed in vitro experiments and edited the manuscript. A.N.B. performed behavioral experiments and edited the manuscript. C.M.M. performed behavioral experiments and edited the manuscript. G.D. assisted in experimental planning and manuscript editing. T.J.P. assisted in experimental planning and manuscript editing. J.D.M. planned, performed, and analyzed in vitro experiments and edited the manuscript. C.L.S. assisted in experimental planning and in writing and editing the manuscript.

Competing interests: The authors have no competing interests to declare with regards to the work contained within this manuscript. T.J.P. and G.D. are cofounders of Ted's Brain Science, PARMedics, and Doloromics. T.J.P. is also a cofounder of 4E Therapeutics and serves as a consultant for Grunenthal and Synerkine Pharma. G.D. is a consultant for Schedule 1 Therapeutics and Psychogenics.

Data and materials availability: All data associated with this study are present in the paper or the Supplementary Materials.

INTRODUCTION

The detection of nonpainful (innocuous) touch and painful (noxious) pressure are critical for all organisms' development, protection, and survival. However, tissue damage or disease can distort touch sensation so that it is no longer beneficial. Instead, innocuous light touch is perceived as painful (mechanical allodynia), painful touch is perceived as more intense, and spontaneous pain arises in the absence of an apparent stimulus (1, 2). The molecular basis of these sensations is not fully understood, and therefore, few adequate, nonaddicting therapies exist. A logical class of therapeutic targets for touch-evoked pain is mechanically-sensitive ion channels that include PIEZO2, a bonafide mechanically-gated innocuous touch transducer, and members of the transient receptor potential (TRP) superfamily including TRPA1 and TRPV4 that contribute to mechanical hypersensitivity (3–9). However, these channels might not be ideal targets for drug development considering that they are also necessary for normal tactile sensation, proprioception, and acute protective pain (10–14). Instead, focus should be placed on proteins that are dispensable for normal tactile and pain sensation but recruited after injury to mediate persistent pain. Here, we identified transient receptor potential canonical 5 (TRPC5) as a previously un-appreciated therapeutic target for injury-related tactile and spontaneous pain. Using pharmacologic and genetic tools, we found that TRPC5 mediates persistent pain after inflammatory and neuropathic injury in mice. We also identified lysophosphatidylcholine (LPC) as an endogenous agonist of both human TRPC5 (hTRPC5) and mouse TRPC5 (mTRPC5) channels and showed that TRPC5 inhibitor efficacy was associated with tissue LPC concentrations after injury. To assess the translational potential of TRPC5 inhibitors, we examined *TRPC5* expression in human dorsal root ganglia (DRG) and found that *TRPC5* is extensively expressed in human sensory neurons. On the basis of these data, we suggest that LPC might be a potential marker for the tailored application of TRPC5 inhibitors, which have high translational potential as non-opioid–based therapies for tactile and spontaneous pain.

RESULTS

TRPC5 activity is required for behavioral mechanical hypersensitivity in persistent pain models

To assess the role of TRPC5 in persistent mechanical allodynia, a battery of inducible pain models was performed in wild-type and global TRPC5 knockout (C5KO) mice. First, intraplantar injection of complete Freund's adjuvant (CFA) was used to induce severe inflammatory pain (Fig. 1A). C5KO mice and wild-type controls developed mechanical allodynia to a similar extent immediately (2 hours) after CFA injection, but C5KO mice started to lose this hypersensitivity 24 hours after injection. Two days after CFA injection, C5KO mice no longer exhibited the mechanical allodynia that persisted for >40 days in wild-type mice (Fig. 1B). C5KO mice also failed to develop hypersensitivity to noxious punctate stimuli (Fig. 1C) or dynamic mechanical allodynia (Fig. 1D) after CFA injection. C5KO mice developed heat hypersensitivity to the same degree as wild-type controls after CFA injection, however (Fig. 1E), demonstrating that global TRPC5 deletion does not generically decrease all peripheral sensation. To model clinical application, we assessed the analgesic efficacy of AC1903, a selective small molecule TRPC5 inhibitor (15), in

established CFA-induced mechanical allodynia. AC1903 eliminated mechanical allodynia in wild-type mice when injected into the inflamed paw 2, 7, or 21 days after CFA injection (Fig. 1F). In addition, AC1903 did not change the mechanical sensitivity of uninjured wild-type mice (Fig. 1, F and G) or injured C5KO mice (Fig. 1G), suggesting that the effects of AC1903 are specific to TRPC5 channel activity, which is not involved in naïve mechanosensation (16). Contralateral administration of AC1903 also had no effect on the mechanical sensitivity of the CFA-injected hindpaw (Fig. 1H), suggesting that inhibitor-related analgesia is mediated by peripherally expressed TRPC5 channels near the site of injury and not by TRPC5 channels expressed in the central nervous system.

Although the CFA model is both reliable and robust, CFA injections lack face validity and may have low translational potential. Therefore, we used the hindpaw incision model of postsurgical pain (17) (Fig. 1I) to determine whether TRPC5 activity contributes to clinically-relevant inflammatory pain. Similar to the CFA model, C5KO and wild-type mice exhibited similar degrees of mechanical allodynia shortly after incision (Fig. 1J). However, C5KO mechanical thresholds were similar to sham mice by postoperative day 5, whereas wild-type thresholds did not recover until postoperative day 7. On postoperative day 4, incised C5KO mice did not exhibit the hypersensitivity to noxious punctate stimuli (fig. S1A) or dynamic brush allodynia (fig. S1B) that was observed in incised wild-type mice. Similar to established CFA mechanical allodynia, established postoperative mechanical allodynia in wild-type mice was alleviated by hindpaw administration of AC1903 and the less selective, more potent TRPC5 antagonist HC-070 (fig. S1, C and D); administration of ML204, a TRPC4/5 antagonist had no effect on postoperative mechanical allodynia. These collective data support the idea that TRPC5 activity contributes to the persistent mechanical hypersensitivity that occurs after peripheral inflammatory injury. The reduced mechanical allodynia observed in C5KO mice did not result from decreased peripheral inflammation because hindpaw swelling was similar between wild-type and C5KO mice after CFA injections (fig. S1E) and hindpaw incision (fig. S1F).

To determine whether TRPC5 is also required for neuropathic mechanical allodynia, spared nerve injury (SNI) and chemotherapy-induced peripheral neuropathy models were used in wild-type and C5KO mice (Fig. 1K). Unlike in the inflammatory models, C5KO and wild-type mice that underwent SNI exhibited persistent mechanical allodynia (Fig. 1L), hypersensitivity to noxious punctate stimuli (fig. S1G), and dynamic brush allodynia (fig. S1H) to a similar extent at all time points after injury. Peripheral AC1903 administration was also ineffective in alleviating SNI-induced mechanical allodynia (fig. S1I). Global C5KO mice, however, failed to develop cold allodynia after SNI (fig. S1J), a finding consistent with previous descriptions of cold-regulating TRPC5 activity (16). The lack of TRPC5 involvement in the mechanical sensitivity associated with this traumatic nerve injury model starkly contrasted channel contributions in inflammatory pain models. To determine whether the lack of TRPC5 involvement in mechanical pain was unique to SNI or more broadly applicable to other neuropathic conditions, C5KO and wild-type mice were treated with paclitaxel, a neurotoxic chemotherapeutic agent that causes profound mechanical hypersensitivity in animal models and patients. Whereas wild-type littermates displayed robust mechanical allodynia (Fig. 1M), hypersensitivity to noxious needle (fig. S1K), and dynamic brush allodynia (fig. S1L), C5KO mice failed to develop any of

these symptoms. Peripheral AC1903 administration also reversed the paclitaxel-induced mechanical allodynia in wild-type mice (fig. S1M), indicating that TRPC5 is required for the maintenance of chemotherapy-induced neuropathy hypersensitivity, similar to what was observed in inflammatory pain models.

Peripheral TRPC5-expressing afferents are exposed to LPC at the site of injury

One potential site of action for TRPC5 inhibitor–related analgesia is peripheral sensory neurons of the dorsal root (16) and trigeminal ganglia (TG) (18). To identify the subclasses of DRG neurons that express *Trpc5*, we performed RNAscope in situ hybridization on tissues isolated from uninjured mice (Fig. 2A). *Trpc5* was expressed in 15% of mouse DRG neurons (Fig. 2B). Similar to previously published single-cell RNA sequencing data (19), *Trpc5* expression was primarily restricted to small-diameter, *P2rx3*-expressing unmyelinated afferents (nonpeptidergic C fibers) and larger-diameter, neurofilament 200 (NF200)–expressing myelinated afferents (Aδ and Aβ fibers) (Fig. 2, C and D).

Although activation of TRPC channels has primarily been attributed to G protein–induced second messenger signaling, we now appreciate that TRPC5 is also activated by stretch in a G protein– independent manner (18, 20). Thus, we hypothesized that injury-specific sensitization of this channel could increase the mechanical sensitivity of select peripheral sensory neurons and underlie the increased behavioral responses to innocuous and noxious touch observed in preclinical injury models. Mechanical hypersensitivity is well documented in C fibers after CFA (8, 21), hindpaw incision (22), SNI (23), and paclitaxel (24) injury, but it is unclear whether this hypersensitivity is mediated by TRPC5. To specifically assess whether peripheral TRPC5 contributes to neuronal mechanical hypersensitivity, ex vivo recordings of tibial nerve C fibers were performed in wild-type and C5KO tissues isolated 7 days after CFA injection (Fig. 3A). Compared to C fibers from wild-type CFA-injected mice, afferents from C5KO CFA-injected mice had elevated mechanical thresholds (Fig. 3, B and C) and reduced firing during dermal force application (Fig. 3, D and E). Mechanical thresholds (fig. S2A) and mechanically induced firing frequencies (fig. S2B) were similar in C fibers isolated from vehicle-treated wild-type and C5KO mice. These ex vivo experiments suggest that peripherally expressed TRPC5 contributes to the persistent mechanical hypersensitivity observed in the CFA model, likely through sensitization or activation of the channel via a chemical mediator present in the injured tissue.

To identify potential mediators, we performed lipid mass spectrometry on the tissues damaged in each of the injury models. LPC (25), a proinflammatory single-chain fatty acid (26), was markedly elevated in the skin of both wild-type and C5KO mice as early as 2 hours after intraplantar CFA injections and for at least seven subsequent days (Fig. 3F; mean LPC concentration in vehicle-treated paws is 63 μM and in CFA-treated paws is 130 μM). Increases were observed in LPC species with varying carbon tail lengths and double-bond number (Table 1). Circulating LPC concentrations were un-changed in CFA-injected animals (fig. S3A and Table 2), suggesting that the excess lipid is derived from cells localized to the injured tissue. Similar injury site–specific increases in LPC were also found in the hindpaw skin of wild-type and C5KO mice 1 and 5 days after incision (Fig. 3G, Tables 1 and 2, and fig. S3B). In contrast to the inflammatory models, total LPC concentration and individual

species quantities were unchanged in the sciatic nerve (Fig. 3H and table S1) or serum (fig. S3C and Table 2) of wild-type or C5KO mice after SNI, perhaps explaining the lack of efficacy of TRPC5 inhibition or deletion in this injury model. After systemic paclitaxel treatment, various LPC species were selectively elevated in the hindpaw skin (Fig. 3I and Table 1), but not in serum (fig. S3D and Table 2) or sciatic nerve (fig. S3E and table S1), closely matching results from the inflammatory models in which TRPC5 inhibitors were analgesic. On the basis of these collective data, LPC may be an endogenous peripheral mediator of TRPC5-dependent mechanical allodynia.

LPC induces TRPC5-dependent neuronal and behavioral mechanical hypersensitivity in mice

After observing injury-induced increases in LPC, we next wanted to determine whether LPC directly contributes to mechanical allodynia. To do this, we administered LPC into the hindpaw of wild-type and C5KO mice. Wild-type mice developed acute mechanical allodynia after LPC injection that was not observed in C5KO mice (Fig. 4A and fig. S4A). We also applied LPC onto the dura mater of wild-type mice to determine whether this lipid contributes to mechanical allodynia in the trigeminal system. Dural injections have been used to induce migraine-like pain in rodents (Fig. 4B)(27). Patients with migraine exhibit mechanical allodynia (28) and have higher concentrations of circulating LPC species (29), but, to our knowledge, a direct relationship between lipid concentrations and mechanical allodynia in these patients has not yet been reported. In wild-type mice, dural infusion of LPC increased the mechanical sensitivity of the periorbital region (Fig. 4C and fig. S4B). However, when LPC was coinfused with AC1903, animals did not develop mechanical allodynia (Fig. 4C). To determine whether this behavioral hypersensitivity resulted from direct neuronal sensitization, we performed whole-cell patch-clamp recordings on TG neurons exposed to LPC (Fig. 4, B and D). LPC increased the amplitude of mechanically-evoked whole-cell currents in wild-type neurons but had no effect on the mechanically-evoked current amplitude of C5KO neurons (Fig. 4, D and E). Further, LPC incubation altered the mechanically-evoked current profiles of wild-type neurons; more slowly adapting (SA) currents were observed when the recording bath contained LPC (Fig. 4F). LPC incubation did not change the mechanical current types observed in C5KO neurons. To summarize, local release of LPC during injury-associated tissue inflammation sensitizes primary afferent responses to mechanical stimulation in a TRPC5-dependent manner.

LPC directly activates murine TRPC5 and induces spontaneous pain

Persistent spontaneous pain is another symptom that develops in many patients after neuropathic and inflammatory injury that is difficult to manage therapeutically. In previous reports, LPC directly activated heterologous hTRPC5 channels in vitro (25). Thus, we hypothesized that if similar activity is occurring at mTRPC5 channels, injury-related LPC increases could drive spontaneous pain in a TRPC5-dependent fashion. To first determine whether LPC directly activates murine TRPC5, LPC-induced calcium flux was measured in human embryonic kidney (HEK) cells stably transfected with mTRPC5. LPC specifically activated mTRPC5 when it was applied up to 32 μM (Fig. 4, G and H, and fig. S6A); when LPC concentrations exceeded 100 μM, nonspecific calcium flux was noted in both transfected and non–TRPC5-transfected HEK cells, likely because of detergent-like

properties of LPC at high concentrations (Fig. 4G). AC1903, the less specific TRPC5 inhibitor HC-070, and the TRPC4/5 inhibitor ML204 (30–32), decreased LPC-induced calcium flux through mTRPC5 (Fig. 4H). These compounds were similarly effective in blocking mTRPC5 activation by (−)-Englerin A, a more selective TRPC-channel agonist (fig. S6B). After demonstrating direct activity of LPC at mTRPC5, we next determined whether the lipid induces spontaneous pain in mice. To assess this behaviorally, we performed conditioned place aversion experiments in wild-type and C5KO mice. In a two-chamber conditioning paradigm, wild-type mice developed a place aversion for the chamber associated with subcutaneous 5 μM LPC administration (Fig. 4I), but not 1 μM LPC (fig. S5A). C5KO mice did not develop the same place aversion as wild-type mice after one (fig. S5B) or 3 days of LPC conditioning (Fig. 4J). To determine whether TRPC5 inhibitors can alleviate established spontaneous pain, we performed conditioned place preference experiments in wild-type mice after paclitaxel treatment (33). For 3 days, animals were conditioned to associate each side of a two-chambered apparatus with the effects of systemic vehicle or HC-070 (3 mg/kg) administration, a dose of TRPC5 inhibitor that alleviates evoked pain-like behaviors in paclitaxel-treated mice (fig. S5C). Unlike vehicle-treated controls, paclitaxel-treated mice developed a preference for the HC-070 chamber (Fig. 4K and fig. S5D).

TRPC5-mediated mechanical hypersensitivity persists after removal of extracellular LPC

Up to this point, our data demonstrate that direct neuronal exposure to LPC induces TRPC5-dependent increases in mechanical sensitivity. To determine whether this hypersensitivity persists in the absence of extracellular LPC, we measured the mechanical sensitivity of TG neurons 48 hours after in vivo application of LPC. Neurons were isolated from wild-type or C5KO mice 24 hours after dural application of LPC, and 24 hours later, mechanical sensitivity was assessed in whole-cell patch-clamp recordings. Neurons from LPC-injected wild-type mice exhibited larger mechanical currents than neurons isolated from LPC-injected C5KO mice or vehicle-injected wild-type animals (Fig. 5A). Similar sensitization was also observed in a behavioral model of migraine-like pain. Migraine attacks can be triggered by subthreshold innocuous stimuli at times when patients are otherwise normal. To determine whether LPC-induced TRPC5 activation and subsequent sensitization in the absence of the lipid contribute to this phenomenon, LPC dural injections were again performed in wild-type and C5KO mice. Similar to Fig. 4C, LPC application induced mechanical allodynia in wildtype mice. After mechanical thresholds recovered, however, subsequent infusion of pH 7.0 synthetic interstitial fluid on the dura induced facial mechanical allodynia in wild-type animals that had previously received an LPC infusion (Fig. 5B). C5KO mice did not develop the initial LPC-induced mechanical allodynia or subsequent pH 7.0–induced hypersensitivity. These data suggest that LPC activation of TRPC5 may be sufficient to induce neuronal and behavioral sensitization that persists even in the absence of the endogenous ligand.

This idea was further confirmed in a transgenic model of sickle cell disease (SCD). SCD mice have higher concentrations of circulating LPC than controls (Fig. 5C and Table 2), likely from disease-related changes in erythrocyte membrane lipid composition (34). AC1903 treatment reduced the behavioral mechanical allodynia (Fig. 5D) and

hypersensitivity to noxious mechanical stimuli (Fig. 5E) observed in SCD mice, paralleling AC1903 efficacy in other models characterized by increased LPC. When SCD DRG neurons were isolated from the LPC-rich native environment, however, AC1903 application still decreased the mechanical sensitivity of these cells. AC1903 incubation increased the number of SCD neurons that were mechanically insensitive in whole-cell patch-clamp experiments while having no effect on neurons isolated from wild-type animals (Fig. 5F). These data suggest that increased TRPC5 activity may persist even in the apparent absence of an endogenous lipid agonist.

TRPC5 is expressed in human sensory neurons and activated by LPC

The analgesic efficacy of TRPC5 inhibitors across seemingly disparate mouse pain models provides rationale for advancing this target to clinical trials. However, it would be remiss to not acknowledge the history of failed targets that were originally characterized as promising analgesics using these exact same animal models (35). One potential reason for this limited translational success is species-specific differences in target expression. To this end, we performed RNAscope in situ hybridization to characterize *TRPC5* expression in human DRG neurons (Fig. 6A and table S2). *TRPC5* expression was observed in 75% of human DRG neurons (Fig. 6B), particularly enriched in medium- and small-diameter neurons [cell bodies <80 μm, roughly equivalent to <40-μm-diameter cell bodies in mouse (Fig. 6C)]. Of the neurons expressing *TRPC5*, ~80% could be classified as nociceptors, coexpressing either calcitonin gene-related peptide CGRP (*CALCA*) or P2X3R (*P2RX3*) (Fig. 6D). The remaining 20% of *TRPC5*-positive neurons did not express either nociceptor marker and are likely part of the Aβ-mechanoreceptor population (36). In addition to verifying expression, we also assessed whether hTRPC5 channels were activated by LPC. Similar to mTRPC5, hTRPC5 activity was specifically induced by physiologically relevant concentrations of LPC (Fig. 6, E and F, and fig. S6C); non-specific, possibly detergent-mediated effects were observed when >100 μM concentration of LPC was applied to cells. Application of AC1903, HC-070, and ML204 effectively blocked both the LPC-induced (Fig. 6F) and (−)-Englerin A-induced (fig. S6D) activation of hTRPC5.

DISCUSSION

Here, we identify TRPC5 as a potential target for persistent tactile and spontaneous pain. Using six different preclinical models, we were able to assess how TRPC5 contributes to pain arising from various pathophysiological sources. Peripheral administration of TRPC5 inhibitors reversed the established mechanical hypersensitivity associated with intraplantar CFA injections, hindpaw incision, paclitaxel treatment, and SCD. Because intraplantar administration of TRPC5 inhibitors was sufficient to alleviate tactile pain, we hypothesized that the anti-allodynic effects of TRPC5 manipulation were mediated by channels expressed in primary sensory afferents. Results from ex vivo and in vitro electrophysiological recordings supported this hypothesis. After CFA injection, C fiber nociceptors from C5KO mice were less sensitive to mechanical stimulation than C fibers isolated from wild-type controls. Similarly, isolated DRG somata from SCD mice were less sensitive to mechanical stimulation when incubating with a TRPC5 inhibitor. However, what was sensitizing TRPC5 across these different pain models? Was there a convergent mediator? Lipid mass

spectrometry revealed tissue-specific increases in LPC, a by-product of phosphatidylcholine metabolism, in all of the pain models that could be alleviated with TRPC5 inhibitors. Although we have not definitively identified the source of LPC in these pain models, one probable source is mast cells that generate LPC as a by-product of prostaglandin synthesis (37). Keratinocytes are another potential source of elevated epidermal LPC. Direct damage to these cells from needle puncture, scalpel cutting, or chemotherapeutics may result in cell lysis and local increases in membrane phospholipids including LPC.

TRPC5-related mechanical allodynia was initiated only after local LPC concentrations were elevated. This lipid-related mechanical hypersensitivity could result through multiple mechanisms. Local increases in LPC, a single fatty acid chain phospholipid, could sensitize mechanically-sensitive ion channels by altering neuronal membrane composition and resulting tension on membrane-embedded proteins. TRPC5 is inherently sensitive to mechanical force (18, 20) and therefore could be directly sensitized through this mechanism. Alternatively, TRPC5 may be a convergent target for second messenger activity that is initiated by other mechanically-gated and mechanically-sensitive plasma membrane ion channels. LPC may also activate mechanically-insensitive proteins, which, through secondary TRPC5 activity, initiate neurogenic inflammation and subsequent behavioral mechanical hypersensitivity; TRPV1-dependent mechanical allodynia is thought to arise through a similar mechanism because the channel itself is not mechanically sensitive (38). Regardless of mechanism, TRPC5 inhibitors effectively alleviated LPC-associated mechanical hypersensitivity that was mediated by sensory neurons within the TG and DRG.

In addition to decreasing tactile pain, TRPC5 inhibitors might also be considered for spontaneous pain management. Here, application of exogenous LPC induced a conditioned place aversion in wild-type mice but had no effect on C5KO mice. In a reciprocal fashion, paclitaxel-treated mice, which exhibit elevated concentrations of LPC, developed a preference for an environment associated with TRPC5 inhibitor treatment. On the basis of these data and the fact that LPC directly induced calcium flux through heterologous mTRPC5 and hTRPC5 channels, we propose that LPC induces spontaneous pain in a TRPC5-dependent manner when sufficiently elevated near sensory afferent terminals. The biochemical basis for this hypothesis is strengthened by recently published cryo–elecrtron microscopy structures of mTRPC5 and hTRPC5 homomers that identified conserved phospholipid binding sites at the interface between individual monomer subunits (30, 39, 40). It is highly likely that additional phospholipids may induce TRPC5-dependent spontaneous pain and mechanical hypersensitivity similar to LPC. Previous reports began to assay the properties of lipids that directly activate hTRPC5 in a G protein–independent fashion, finding that activity profiles were specific to both the polar head group and carbon tail length (25, 41). Characterizing the full complement of endogenous TRPC5 lipid agonists will only further expand the list of conditions for which TRPC5 inhibitors may prove analgesic.

After the successful application of TRPC5 inhibitors in our pre-clinical models, we assessed TRPC5's translational potential by using human tissues and expressing the human channel in a heterologous system. We observed uniform *TRPC5* expression in DRG tissue from three different donors; *TRPC5* was expressed in 75% of soma, most of which are putative

nociceptors. To our knowledge, the human DRG used in these studies were obtained from donors who did not suffer from chronic pain, and the mouse DRG used in our RNAscope experiments were obtained from naïve animals. Therefore, *TRPC5* expression may be underreported in our experiments because channel expression is likely temporally and spatially regulated by LPC. In previous studies, elevated LPC increased TRPC5 expression and trafficking to the plasma membrane of endothelial cells (42) where the channel could be subsequently activated by mechanical stimuli, G protein signaling, or endogenous agonists like protons and other phospholipids (43, 44). Future studies should determine whether a similar phenomenon occurs in sensory neurons and if membrane localization remains elevated after LPC concentrations normalize. If the latter is true, this could partially explain why TRPC5 inhibitors effectively alleviate mechanical hypersensitivity in mice in the apparent absence of LPC.

In the three human donor tissues, the expression profile of *TRPC5* was nearly identical to that observed for *TRPV1*, a high-priority clinical target; first-generation TRPV1 inhibitors were deemed unsuccessful when patients developed hyperthermia (45), but second-generation compounds effectively decreased osteoarthritis pain and are now in phase 3 clinical trials (46). Because the expression profile of *TRPC5* is just as wide as *TRPV1*, it is possible that compounds targeting these channels may be effective if administered for the appropriate indications. TRPC5 inhibitors may prove analgesic in all of the following conditions in which LPC is elevated: rheumatoid arthritis (47), osteoarthritis (48), SCD (34), fibromyalgia (49), diabetes (50), multiple sclerosis (47), primary dysmenorrhea (51), lumbar spinal stenosis (52), and migraine (29). Additional support for TRPC5 inhibitors in migraine comes from a recent study in which *Trpc5* expression was elevated in TG neurons of mice that developed pituitary adenylate cyclase activating polypeptide (PACAP)–induced light aversion (53). Future studies should determine whether TRPC5 is a convergent secondary target for the G protein–coupled peptidergic signaling (CGRP and PACAP) (54) that occurs in patients with migraine.

Two TRPC5 inhibitors recently completed phase 1 clinical trials; compounds GFB-887 and BI 1358894, originally developed for kidney disease and affective disorders, respectively, are advancing to phase 2 trials because both compounds were well tolerated by phase 1 participants (www.clinicaltrials.gov). The widespread expression of TRPC5 presents several limitations when considering the translational potential of TRPC5 inhibitors. Results from our patch-clamp recordings suggest that mechanical hypersensitivity is mediated, at least in part, by TRPC5 channels expressed in peripheral sensory neurons. These data do not exclude the possibility, however, that central or non-neuronal expression of TRPC5 also contributes to this sensation. TRPC5 is expressed in many endothelial (55) and epithelial cells including kidney podocytes (15), fibroblast-like synoviocytes in joints (56), and epidermal keratinocytes (57). Keratinocyte activity is not only necessary for normal responses to both innocuous and noxious mechanical stimuli (58) but also capable of inducing firing in closely juxtaposed sensory neuron terminals (59). It is very possible, therefore, that direct or indirect activation of TRPC5 in these cells may sensitize mechanotransduction mechanisms even before the first neuronal synapse, thus potentially confounding data interpretation in behavioral assays or teased fiber recordings. Previously, TRPC5 activity in synoviocytes was associated with better outcomes in a rodent model of

arthritis; when compared to wildtype controls, C5KO mice exhibited increased inflammatory markers in the synovium after intra-articular injection of CFA (56). In our experiments, C5KO and wild-type mice exhibited the same extent of hindpaw swelling after intraplantar CFA injection. C5KO mice also exhibited less mechanical allodynia than controls after intraplantar CFA injection, but when CFA was injected into the knee, C5KO mice exhibited more referred and secondary mechanical allodynia than wild-type animals (56). These discrepancies may result from activation of TRPC5 in select populations of non-neuronal cells. We used both localized and widespread injury models in our study, and although the anti-allodynic effects of TRPC5 inhibitors or knockdown were conserved across these models, it is possible that additional tissue-specific injuries, like those incurred in arthritis models, may result in differential effects of TRPC5 manipulation. One of the ongoing TRPC5 inhibitor clinical trials is for use in kidney disease. Inhibition or knockdown of TRPC5 protects against podocyte loss in two different rat models of kidney disease, and no adverse effects of chronic inhibitor administration were noted in naïve animals; AC1903-treated healthy rats exhibited normal body weight, blood pressure, and kidney function (15). Considered with the relatively normal phenotype observed in naïve C5KO mice (60), these results suggest that on-target side effects of TRPC5 inhibitors will likely not impede successful translational application of these compounds. The second ongoing TRPC5 inhibitor clinical trial is for use in affective disorders. The anxiolytic effects of TRPC5 inhibitors are proposedly mediated by TRPC5 expression in the amygdala (60). In amygdala neurons, TRPC5 is primarily activated by G protein signaling. The same GPCRs that result in TRPC5 activation, namely, group I metabotropic glutamate receptors (60), are also involved in the top-down induction of mechanical allodynia (61) and visceral pain (62). Therefore, when administered systemically, TRPC5 inhibitors may alleviate pain to a greater extent by modulating both the sensory discriminative aspects of pain conferred by TRPC5 channels in the peripheral nervous systems and the affective aspects of pain, which may be mediated by centrally expressed TRPC5.

MATERIALS AND METHODS

Study design

The overall objective of this study was to assess the extent to which TRPC5 contributes to persistent mechanical and spontaneous pain in rodent models. To achieve this, we performed reflexive and operant behavioral tests in inducible and genetic mouse models of persistent inflammatory and/or neuropathic pain. To identify the anatomical sites in which TRPC5 expression contributes to persistent pain, we performed in vitro and ex vivo electrophysiological recordings on mouse tissues. Expression in human tissues was confirmed with RNAscope, and ligand–hTRPC5 channel interactions were assayed in a heterologous expression system. Lipid mass spectroscopy was also used to measure endogenous ligand concentrations in various mouse tissues, the specific actions of which were confirmed in heterologous expression systems. Sample sizes were determined on the basis of previous behavioral, electrophysiological, and molecular data published by our laboratories. In all experiments, animals and cell lines were randomly assigned to treatment groups. Experimenters were blinded to genotype, drug treatment, and/or injury model during data acquisition and analysis; it is impossible to blind injury model in CFA

or hindpaw incision behaviors, but experimenter was blinded to genotype and/or drug treatment. Biological replicate number is noted in all figure legends; biological and technical replicates are noted for TRPC5 cell line experiments.

Animals

TRPC5 knockout (C5KO) (63), 129;S1 (C5KO wild-type), C57BL/6, Berkley SS (SCD) (64), and B6;129 (SCD wild-type) mice were bred in house and maintained on a 14-hour light/10-hour dark schedule with ad libitum access to rodent chow and water. Equally sized cohorts of male and female mice aged 8 to 26 weeks were used; 6- to 8-week-old animals were used for dural injections. All protocols were in accordance with the National Institutes of Health guidelines and were approved by the Institutional Animal Care and Use Committee at the Medical College of Wisconsin (Milwaukee, WI; protocol no. 383).

Injury models

CFA injections—Thirty microliters of stock CFA (8, 65) or sterile phosphate-buffered saline (PBS) was injected into the plantar aspect of one hindpaw.

Hindpaw plantar incision—Postoperative pain was modeled using the hindpaw plantar incision procedure (22, 66). Animals were maintained on inhalable isoflurane (1.5%) for the duration of the procedure (< 10 min). Starting 2 mm from the proximal edge of the heel, a 5-mm longitudinal incision was made through the glabrous skin. The underlying plantaris muscle was exposed, raised to rest on the tips of curved forceps, and then incised longitudinally along the entire exposed length. The muscle was then repositioned, two sutures were used to close the incised skin, and bacitracin was applied to incision. Sham animals were anesthetized and had bacitracin applied to one hindpaw.

Spared tibial nerve injury—A modified version of the SNI model (67) was used to model neuropathic pain. Animals were maintained on inhalable isoflurane (1.5%) for the duration of the procedure (<15 min). After incising the lateral skin of the thigh, the biceps femoris muscle was manipulated to expose the three distal branches of the sciatic nerve. The sural and common peroneal branches were ligated just distal to the branch point and transected 2 to 4 mm distal to the ligation; the tibial nerve was not ligated or cut. The overlying muscles were repositioned, and the skin incision was closed with staples. In sham animals, all branches of the sciatic nerve were exposed but not ligated or cut.

Paclitaxel treatment—Paclitaxel (Taxol) was dissolved in vehicle (16% ethanol, 16% Cremophor, and 68% saline) to achieve a working solution of 0.8 mg/ml. Paclitaxel (8 mg/kg) or vehicle was injected intraperitoneally every other day over 8 days.

Dural injections—Dural injections were performed as previously described (27). Animals (≤8 weeks of age) were maintained on inhalable isoflurane (1.5%) for the duration of the procedure (<5 min). A 0.5-mm cannula was inserted through the soft tissue at the junction of the sagittal and lambdoid sutures; 5 μl of LPC, LPC + AC1903, or pH 7.0 saline was infused through the cannula.

Behavioral tests

For all reflexive behavioral tests, animals were habituated to testing chamber and experimenter presence for >1 hour (68). Experimenter was blinded to genotype, drug treatment, and/or injury model where applicable. Animals were randomly assigned to treatment groups.

von Frey mechanical allodynia testing—Hindpaw sensitivity to punctate mechanical stimulation was assessed via calibrated von Frey filaments (0.20 to 13.73 mN) and the up-down assessment method as previously described (69, 70). The 50% withdrawal threshold was calculated for each paw as previously described (71). Toe flaring without paw withdrawal was not considered a response. Calibrated von Frey filaments were also used to assess facial sensitivity to punctate mechanical stimulation as previously described (27). Animals habituated to testing chambers (acrylic cups, 6.5 cm in diameter by 7.0 cm in height) for 2 hours on each day of the 2 days before start of testing. The 50% withdrawal threshold was calculated using the same analysis used for hindpaw measurements.

Noxious needle testing—Hindpaw sensitivity to noxious punctate mechanical probing was assessed via needle stimulation as previously described (72). A 25-gauge needle was pressed into the center of each hindpaw with enough force to indent but not puncture the skin. Each paw was stimulated 10 times, and the response frequency and characterization were recorded. Responses were characterized as null (no paw withdrawal), innocuous (simple withdrawal), or noxious (withdrawal accompanied by biting, licking, flicking, or additional attending to the paw).

Paintbrush testing—Hindpaw sensitivity to dynamic light touch was assessed via paint-brush stimulation as previously described (73). A fine horsehair paintbrush was swept across the plantar surface of each hindpaw from heel to toe pads, keeping the speed and force about constant between applications. Each paw was stimulated 10 times, and the response frequency and characterization were reported as described in needle testing.

Conditioned place aversion—A 5- or 3-day protocol was used to assess the nonreflexive perception of LPC treatment. On preconditioning day, mice were placed into a two-chamber box. Individual chambers of the box could be visually differentiated by wall coverings (chamber 1: white polka dots on black background and chamber 2: equally sized black and white stripes on 30° diagonal). Chambers were connected via a retractable door. Each box was housed in a custom-built closed chamber fitted with a small circulating fan, white light-emitting diode light strips, and overhead camera. Mice were allowed to freely move between the two chambers for 15 min. Animal movements were recorded by the overhead cameras, and the total time spent in each chamber was analyzed with ANY-maze software. Animals spending <20 or >80% of the total trial in one of the two chambers were removed from the experiment on grounds of initial chamber bias (74). Conditioning was completed in a biased fashion (75, 76). In morning training sessions, all animals received a subcutaneous vehicle injection [1× PBS (pH 7.4); same volume as LPC injection] and were then immediately placed into their more preferred chamber from day 1 for 30 min. Animal movement was restricted to one chamber via the retractable door. In afternoon

training sessions, all animals received subcutaneous injections of 1 or 5 μM LPC and were then immediately placed into their less preferred chamber from day 1 for 30 min. On postconditioning day 5, mice were again placed into the box and allowed to freely move between the two chambers for 15 min. Total time in each chamber on day 5 was recorded, and differences between pre- and postconditioning times in each chamber were analyzed.

Analgesic conditioned place preference—Animals were placed through a 5-day analgesic conditioned place preference (aCPP) protocol 17 days after the first paclitaxel or vehicle injection. The 5-day protocol was identical to conditioned place aversion experiments save the following changes: (i) In the morning training sessions, all animals orally received ~200 μl of 0.5% methyl cellulose 45 min before being placed into their more preferred chamber. (ii) In the afternoon training sessions, all animals orally received HC-070 (3 mg/kg) 45 min before being placed into their less preferred chamber.

Paw edema measurements—Animals were anesthetized with inhalable isoflurane (1.5%), and the diameter of the tallest part of the paw was measured with digital calipers.

Electrophysiology

Ex vivo teased tibial nerve recordings—Teased fiber tibial nerve recordings were completed as previously described (58, 77). Seven days after CFA or vehicle injection, animals were anesthetized and then euthanized via cervical dislocation. The glabrous skin and tibial nerve from one leg were dissected and placed in a bath containing heated (32° ± 0.5°C), oxygenated buffer (pH of 7.45 ± 0.05) consisting of 123 mM NaCl, 3.5 mM KCl, 2.0 mM $CaCl_2$, 0.7 mM $MgSO_4$, 1.7 mM NaH_2PO_4, 5.5 mM glucose, 7.5 mM sucrose 9.5 mM sodium gluconate, and 10 mM Hepes. The nerve was placed into an adjacent chamber of the bath filled with mineral oil and then teased into small bundles that were individually placed on a silver wire electrode. Mechanically responsive receptive fields were identified by probing the corium with a blunt glass rod. For these experiments, activity was only recorded in mechanically responsive C fibers [conduction velocity < 1.2 m/s (78)]. Thresholds for mechanically induced action potential firing were determined using a custom-built, feedback-controlled mechanical stimulator that applied a continuous force ramp from 0 to 100 mN. Firing frequencies were recorded during static force applications (2, 5, 10, 20, 40, 100, 150, and 200 mN for 10 s; 1 min interforce interval). All data were recorded and analyzed in LabChart software. Experimenter was blinded to genotype until data analysis was complete.

DRG and TG neuronal cultures—Mice were euthanized, and sensory neurons were isolated from bilateral lumbar 1 to 6 ganglia or the bilateral TG; culturing procedures were identical for both tissues. Ganglia were incubated with collagenase type IV (1 mg/ml) for 40 min at 37°C and 5% CO_2 and then 0.05% trypsin for 45 min. Ganglia were mechanically dissociated and plated onto laminin-coated glass coverslips. Two hours after plating, neurons were fed with Dulbecco's modified Eagle's medium (DMEM)/Ham's F12 medium supplemented with 10% heat-inactivated horse serum, 2 mM L-glutamine, 1% glucose, penicillin (100 U/ml), and streptomycin (100 μg/ml). Neurons grew overnight at 37°C and 5% CO_2.

Whole-cell patch clamping—Coverslips were placed onto a Nikon Eclipse TE200 inverted microscope. Cells were continuously superfused with room temperature extracellular normal Hepes solution (pH 7.4 ± 0.05 and 310 ± 3 mOsm) containing 140 mM NaCl, 2.8 mM KCl, 2 mM $CaCl_2$,1 mM $MgCl_2$, 10 mM Hepes, and 10 mM glucose. Neurons (holding voltage −70 mV) were patch-clamped in voltage clamp mode with borosilicate glass pipettes filled with intracellular normal Hepes solution (pH 7.20 ± 0.05 and 290 ± 3 mOsm) containing 135 mM KCl, 10 mM NaCl, 1 mM $MgCl_2$, 1 mM EGTA, 0.2 mM NaGTP, 2.5 mM $ATPNa_2$, and 10 mM Hepes. Cell capacitance and series resistance were kept below 10 megohm for all cell types. When using DRG cultures, only small-diameter neurons (<27 μM, putative nociceptors) were recorded. Cell membranes were mechanically displaced (1.7 of 1.7 μm/V for 200 ms; 3 min intertrial interval) by a second borosilicate glass pipette driven by a piezo stack actuator (pipette velocity, 106.25 μm/ms). All data were recorded in Pulse software. Current amplitude and type were analyzed in Fit Master software as previously described (65). Current density was quantified by correcting the peak current amplitude at a given indentation by the capacitance of that neuron; graphs include the current density of all mechanically sensitive neurons, regardless of current profile subclass. Current profiles were classified using the following parameters: rapidly adapting (RA) inactivation time constant (τ) < 10 ms, intermediate adapting (IA) 10 < τ < 30 ms, SA τ > 30 ms. The mechanical threshold was designated as the first stimulation that elicited >20 pA inward current; mechanically insensitive cells were mechanically stimulated at least three times and did not exhibit an inward current >20 pA during any stimulation. Cells were only included if the leak current stayed below 200 pA for three or more mechanical stimulations. For in vitro LPC or AC1903 experiments, neurons were exposed to chemical for a minimum of 5 min and a maximum of 1.5 hours. Experimenter was blinded to genotype and treatment until data analysis was complete.

Lipid mass spectrometry

Tissue preparation—Hindpaw plantar skin was dissected 2 hours or 7 days after CFA injection, 1 or 5 days after incision, and 21 days after the first paclitaxel injection. Sciatic nerve was isolated 10 days after SNI or 21 days after the first paclitaxel injection. Tissues were immediately frozen on dry ice after isolation. Serum was collected from all injury models at the same time points as follows: Blood was obtained via cardiac puncture from deeply anesthetized mice. Blood was centrifuged at 1500 rpm, 4°C, for 15 min. Serum was pipetted into sterile tube and then immediately frozen on dry ice. Samples were then shipped to the Northwest Metabolomics Research Center for further processing.

Sample preparation—Lipids were extracted from samples as previously described (79). Samples were reconstituted in 250 μl of Lipidyzer running buffer composed of dichloromethane:methanol with 10 mM ammonium acetate.

Mass spectrometry—Quantitative lipidomics was performed with the Sciex Lipidyzer platform consisting of Shimadzu Nexera X2 LC-30 AD pumps, a Shimadzu Nexera X2 SIL-30 AC autosampler, and a Sciex QTRAP 5500 mass spectrometer equipped with SelexION for differential mobility spectrometry (DMS). 1-Propanol was used as the chemical modifier for the DMS. Samples were introduced to the mass spectrometer by flow

injection analysis at 8 μl/min. Lipids were analyzed in negative electrospray ionization mode using multiple reaction monitoring. A total of 26 LPC lipids were targeted in the analysis.

Data processing—Data were acquired and processed using Analyst 1.6.3 and Lipidomics Workflow Manager 1.0.5.0. Stucky Laboratory members analyzed the data in a blinded fashion.

TRPC5 stable–cell line generation and Fluo-4 calcium flux assays

Stable cell lines were generated in HEK293 (American Type Culture Collection, mycoplasma-free) using a pCMV vector expressing either 1 μg of mTRPC5 or hTRPC5 (Origene) cotransfected with 7 μg of pBabe Puro vector for rapid stable selection. Cell lines were selected and maintained DMEM containing 10% fetal bovine serum (FBS), puromycin (5 μg/ml; GoldBio), and G418 (750 μg/ml; GoldBio). On the day before assay, cells were seeded into 384-well poly-L-lysine–coated black plates at a density of 10,000 cells per well in DMEM containing 1% dialyzed FBS. On the day of the assay, media were decanted, and the cells were incubated with Fluo-4 Direct dye (Invitrogen, 20 μl per well) for 1 hour at 37°C, which was reconstituted in drug buffer in a 1:10 dilution [20 mM Hepes-buffered Hanks' balanced salt solution (HBSS) (pH 7.4)] containing 2.5 mM probenecid. After dye load, cells were allowed to equilibrate to room temperature for 15 min and then placed in a FLIPR^{TETRA} fluorescence imaging plate reader (Molecular Dynamics). Ligand dilutions were prepared at 5× final concentration in drug buffer [20 mM Hepes-buffered HBSS (pH 7.4)] containing 0.1% bovine serum albumin (BSA) and 0.01% ascorbic acid, final concentration. Ligand dilutions were aliquoted into 384-well plastic plates and placed in the FLIPR^{TETRA} for drug stimulation. For competition antagonist assays, plates were challenged with either LPC (32 to 60 μM) or (−)-Englerin A (100 nM) and prepared at 6× final concentration in drug buffer [20 mM Hepes-buffered HBSS (pH 7.4)] containing 0.1% BSA and 0.01% ascorbic acid, final concentration. Fluorescence for the FLIPR^{TETRA} was programmed to read baseline fluorescence for 10 s (1 read/s), and afterward, 5 μl of drug per well was added and read for a total of 5 min (1 read/s). Fluorescence in each well was normalized to the average of the first 10 reads for baseline fluorescence, and then the area under the curve (AUC) was determined and calculated. AUC was plotted as a function of ligand concentration, and data were analyzed as nonlinear regression using "log(agonist) vs. response— variable slope" in GraphPad Prism 5.0 to yield Emax (Efficiency max) and median effective concentration parameter estimates.

Chemical matter—AC1903 [provided by C. Hopkins (15); 2.5 μg/μl] was gently heated in 10% EtOH, 40% polyethylene glycol (molecular weight 400), and 50% saline vehicle until dissolved. LPC was purchased from Sigma-Aldrich and dissolved in 0.02% EtOH vehicle. ML204 was purchased from Sigma-Aldrich and dissolved in 12.5% dimethyl sulfoxide (DMSO) vehicle. HC-070 was purchased from MedChemExpress and dissolved in 0.125% DMSO vehicle for intraplantar injections or suspended in 0.5% methyl cellulose for systemic administration (31). (−)-Englerin A was purchased from Sigma-Aldrich (80). For in vitro experiments, all compounds were dissolved in DMSO at 100 mM, except LPC was dissolved in ethanol.

RNAscope

Tissue preparation—All human tissue procurement procedures were approved by the Institutional Review Boards at the University of Texas at Dallas. Human DRGs (L5) were collected, frozen on dry ice, and stored in a −80°C freezer. Donor information is provided in table S2. The human DRGs were gradually embedded with optimal cutting temperature (OCT) in a cryomold by adding small volumes of OCT over dry ice to avoid thawing. C57BL/6 mice (two female and one male) were decapitated under isoflurane, and the lumbar DRGs were immediately dissected and frozen in OCT in a cryomold over dry ice. All tissues were cryostat-sectioned at 20 μm onto Super-Frost Plus charged slides. Sections were only briefly thawed to adhere to the slide but were immediately returned to the −20°C cryostat chamber until completion of sectioning. The slides were then immediately used for histology.

RNAscope in situ hybridization—RNAscope in situ hybridization multiplex version 1 was performed as instructed by Advanced Cell Diagnostics (ACD). Slides were removed from the cryostat and immediately transferred to cold (4°C) 10% formalin for 15 min. The tissues were then dehydrated in 50% ethanol (5 min), 70% ethanol (5 min), and 100% ethanol (10 min) at room temperature. The slides were air-dried briefly, and then boundaries were drawn around each section using a hydrophobic pen (ImmEdge PAP pen, Vector Laboratories). When hydrophobic boundaries had dried, protease IV reagent was added to each section until fully covered and incubated for 2 to 5 min at room temperature. The protease IV incubation period was optimized for the specific lot of protease IV reagent and for each DRG as recommended by ACD. Mouse DRGs were incubated for 1 min in protease IV. Slides were washed briefly in 1× PBS (pH 7.4) at room temperature. Each slide was then placed in a prewarmed humidity control tray (ACD) containing dampened filter paper, and a 50:1:1 dilution (as directed by ACD because of stock concentrations) of *TRPC5* (human: ACD catalog no. 427651; channel 1; mouse: ACD catalog no. 476241; channel 1), *CALCA* (human: ACD catalog no. 605551; channel 2; mouse: 417961), and *P2RX3* (human: ACD catalog no. 406301; channel 3; mouse: ACD catalog no. 521611) was pipetted onto each section until fully submerged. This was performed one slide at a time to avoid liquid evaporation and section drying. The humidity control tray was placed in a HybEZ oven (ACD) for 2 hours at 40°C. After probe incubation, the slides were washed two times in 1× RNAscope wash buffer and returned to the oven for 30 min after submersion in AMP-1 reagent. Washes and amplification were repeated using AMP-2, AMP-3, and AMP-4 reagents with a 15-, 30-, and 15-min incubation period, respectively. AMP-4 ALT C (channel 1 = Atto 550, channel 2 = Atto 647, and channel 3 = Alexa 488) was used for all experiments. Slides were then washed two times in 0.1 M phosphate buffer (PB, pH7.4). Human slides were incubated in 4′,6-diamidino-2-phenylindole (DAPI) (1:5000) in 0.1 M PB for 1 min before being washed, air-dried, and coverslipped with Pro-Long Gold Antifade mounting medium. Given the nonspecificity for NF200 in human DRG (81), immunohistochemistry for NF200 was only conducted on mouse tissues. After completion of RNA-scope in situ hybridization, mouse slides were incubated in blocking buffer (10% normal goat serum and 0.3% Triton X-100 in 0.1 M PB) for 1 hour at room temperature while being shielded from light. Slides were placed in a light-protected humidity-controlled tray and incubated in primary antibody (mouse anti-NF200; clone N52; Sigma-Aldrich) at

1:500 in blocking buffer overnight at 4°C. The next day, slides were washed two times in 0.1 M PB and then incubated in secondary antibody (goat anti-mouse H&L 405; 1:2000) for 1 hour at room temperature. Sections were washed two times in 0.1 M PB, air-dried, and coverslipped with ProLong Gold Antifade mounting medium.

Tissue quality check—All human and mouse DRGs were checked for RNA quality by using a positive control probe cocktail (ACD) that contains probes for high-, medium-, and low-expressing mRNAs that are present in all cells (ubiquitin C > peptidyl-prolyl cis-trans isomerase B > DNA-directed RNA polymerase II subunit RPB1). DRGs that showed signal for all three positive control probes were used to generate experimental data. A negative control probe against the bacterial DapB gene (ACD) was used to check for nonspecific/background label.

Image analysis—DRG sections were imaged on an Olympus FV3000 confocal microscope at ×20 magnification. Three to four 20× images were acquired of each human DRG section, and three sections were imaged per human donor. One 20× image was acquired of each mouse DRG section, and two to three sections were imaged per mouse. The acquisition parameters were set on the basis of guidelines for the FV3000 provided by Olympus. In particular, the gain was kept at the default setting 1, HV ≤ 600, offset = 4, and laser power ≤ 15%. The raw image files were brightened, contrasted, and pseudo-colored in Olympus CellSens software (v1.18) and then analyzed manually one cell at a time for expression of each gene target. Cell diameters were measured using the polyline tool. Total neuron counts for human samples were acquired by counting all of the probe-labeled neurons and all neurons that were clearly outlined by DAPI (satellite cell) signal and contained lipofuscin in the overlay image. For mouse, the total number of neurons was calculated by summing all NF200-, *Calca*-, and *P2rx3*-positive neurons.

In the human samples, large globular structures and/or signal that autofluoresced in all three channels (488, 550, and 647; appears white in the overlay images) was considered to be background lipofuscin and was not analyzed. Aside from adjusting brightness/contrast, we performed no digital image processing to subtract background. We attempted to optimize automated imaging analysis tools for our purposes, but these tools were designed to work with fresh, low-background rodent tissues, not human samples taken from older organ donors. As such, we chose to implement a manual approach in our imaging analysis in which we used our own judgment of the negative/positive controls and target images to assess mRNA label. Images were not analyzed in a blinded fashion.

Statistical analysis

Individual data points were presented whenever possible in addition to group means ± SEM. Data were analyzed using GraphPad Prism 8; results were considered statistically significant when $P < 0.05$. For behavioral experiments, data from each sex were independently analyzed. No significant differences were noted, so data were reanalyzed with sexes combined.

Supplementary Material

Refer to Web version on PubMed Central for supplementary material.

Acknowledgments:

We thank C. Hopkins for providing AC1903, A. Menzel for technical assistance, the laboratory of E. Lumpkin for technical advice, D. Clapham for comments on the manuscript, the Neuroscience Research Center at the Medical College of Wisconsin for access to behavioral equipment, and the Northwest Metabolomics Research Center for lipid mass spectrometry services.

Funding:

This work was funded by NIH grants NS106789 to K.E.S., NS040538 to C.L.S., NS070711 to C.L.S., NS108278 to C.L.S., NS104200 to G.D., NS0655926 to T.J.P., and 1S10OD021562–01 to the Northwest Metabolomics Research Center, startup funds to J.D.M., and the Research and Education Initiative Fund, a component of the Advancing a Healthier Wisconsin Endowment at the Medical College of Wisconsin.

REFERENCES AND NOTES

1. Lolignier S, Eijkelkamp N, Wood JN, Mechanical allodynia. Pflugers Arch 467, 133–139 (2014). [PubMed: 24846747]
2. Woolf CJ, Central sensitization: Implications for the diagnosis and treatment of pain. Pain 152, S2–S15 (2011). [PubMed: 20961685]
3. Eid SR, Crown ED, Moore EL, Liang HA, Choong KC, Dima S, Henze DA, Kane SA, Urban MO, HC-030031, a TRPA1 selective antagonist, attenuates inflammatory- and neuropathy-induced mechanical hypersensitivity. Mol. Pain 4, 48 (2008). [PubMed: 18954467]
4. Szczot M, Liljencrantz J, Ghitani N, Barik A, Lam R, Thompson JH, Bharucha-Goebel D, Saade D, Necaise A, Donkervoort S, Foley AR, Gordon T, Case L, Bushnell MC, Bönnemann CG, Chesler AT, PIEZO2 mediates injury-induced tactile pain in mice and humans. Sci. Transl. Med 10, eaat9892 (2018). [PubMed: 30305456]
5. Murthy SE, Loud MC, Daou I, Marshall KL, Schwaller F, Kühnemund J, Francisco AG, Keenan WT, Dubin AE, Lewin GR, Patapoutian A, The mechanosensitive ion channel Piezo2 mediates sensitivity to mechanical pain in mice. Sci. Transl. Med 10, eaat9897 (2018). [PubMed: 30305457]
6. Kwan KY, Allchorne AJ, Vollrath MA, Christensen AP, Zhang DS, Woolf CJ, Corey DP, TRPA1 contributes to cold, mechanical, and chemical nociception but is not essential for hair-cell transduction. Neuron 50, 277–289 (2006). [PubMed: 16630838]
7. Petrus M, Peier AM, Bandell M, Hwang SW, Huynh T, Olney N, Jegla T, Patapoutian A, A role of TRPA1 in mechanical hyperalgesia is revealed by pharmacological inhibition. Mol. Pain 3, 40 (2007). [PubMed: 18086313]
8. Lennertz RC, Kossyreva EA, Smith AK, Stucky CL, TRPA1 mediates mechanical sensitization in nociceptors during inflammation. PLOS ONE 7, e43597 (2012). [PubMed: 22927999]
9. Dunham JP, Kelly S, Donaldson LF, Inflammation reduces mechanical thresholds in a population of transient receptor potential channel A1-expressing nociceptors in the rat. Eur. J. Neurosci 27, 3151–3160 (2008). [PubMed: 18598259]
10. Coste B, Mathur J, Schmidt M, Earley TJ, Ranade S, Petrus MJ, Dubin AE, Patapoutian A, Piezo1 and Piezo2 are essential components of distinct mechanically activated cation channels. Science 330, 55–60 (2010). [PubMed: 20813920]
11. Chesler AT, Szczot M, Bharucha-Goebel D, Čeko M, Donkervoort S, Laubacher C, Hayes LH, Alter K, Zampieri C, Stanley C, Innes AM, Mah JK, Grosmann CM, Bradley N, Nguyen D, Foley AR, Le Pichon CE, Bönnemann CG, The role of *PIEZO2* in human mechanosensation. N. Engl. J. Med 375, 1355–1364 (2016). [PubMed: 27653382]
12. Kerstein PC, del Camino D, Moran MM, Stucky CL, Pharmacological blockade of TRPA1 inhibits mechanical firing in nociceptors. Mol. Pain 5, 19 (2009). [PubMed: 19383149]

13. Kwan KY, Glazer JM, Corey DP, Rice FL, Stucky CL, TRPA1 modulates mechanotransduction in cutaneous sensory neurons. J. Neurosci 29, 4808–4819 (2009). [PubMed: 19369549]
14. Zappia KJ, O'Hara CL, Moehring F, Kwan KY, Stucky CL, Sensory neuron-specific deletion of TRPA1 results in mechanical cutaneous sensory deficits. eNeuro 4, ENEURO.0069–16.2017 (2017).
15. Zhou Y, Castonguay P, Sidhom EH, Clark AR, Dvela-Levitt M, Kim S, Sieber J, Wieder N, Jung JY, Andreeva S, Reichardt J, Dubois F, Hoffmann SC, Basgen JM, Montesinos MS, Weins A, Johnson AC, Lander ES, Garrett MR, Hopkins CR, Greka A, A small-molecule inhibitor of TRPC5 ion channels suppresses progressive kidney disease in animal models. Science 358, 1332–1336 (2017). [PubMed: 29217578]
16. Zimmermann K, Lennerz JK, Hein A, Link AS, Kaczmarek JS, Delling M, Uysal S, Pfeifer JD, Riccio A, Clapham DE, Transient receptor potential cation channel, subfamily C, member 5 (TRPC5) is a cold-transducer in the peripheral nervous system. Proc. Natl. Acad. Sci. U.S.A 108, 18114–18119 (2011). [PubMed: 22025699]
17. Brennan TJ, Vandermeulen EP, Gebhart GF, Characterization of a rat model of incisional pain. Pain 64, 493–502 (1996). [PubMed: 8783314]
18. Gomis A, Soriano S, Belmonte C, Viana F, Hypoosmotic- and pressure-induced membrane stretch activate TRPC5 channels. J. Physiol 586, 5633–5649 (2008). [PubMed: 18832422]
19. Usoskin D, Furlan A, Islam S, Abdo H, Lönnerberg P, Lou D, Hjerling-Leffler J, Haeggström J, Kharchenko O, Kharchenko PV, Linnarsson S, Ernfors P, Unbiased classification of sensory neuron types by large-scale single-cell RNA sequencing. Nat. Neurosci 18, 145–153 (2015). [PubMed: 25420068]
20. Shen B, Wong C-O, Lau OC, Woo T, Bai S, Huang Y, Yao X, Plasma membrane mechanical stress activates TRPC5 channels. PLOS ONE 10, e0122227 (2015). [PubMed: 25849346]
21. Weyer AD, Zappia KJ, Garrison SR, O'Hara CL, Dodge AK, Stucky CL, Nociceptor sensitization depends on age and pain chronicity. eNeuro 3, ENEURO.0115–15.2015 (2016).
22. Cowie AM, Menzel AD, O'Hara C, Lawlor MW, Stucky CL, NOD-like receptor protein 3 inflammasome drives postoperative mechanical pain in a sex-dependent manner. Pain 160, 1794–1816 (2019). [PubMed: 31335648]
23. Smith AK, O'Hara CL, Stucky CL, Mechanical sensitization of cutaneous sensory fibers in the spared nerve injury mouse model. Mol. Pain 9, 61 (2013). [PubMed: 24286165]
24. Shim HS, Bae C, Wang J, Lee K-H, Hankerd KM, Kim HK, Chung JM, La J-H, Peripheral and central oxidative stress in chemotherapy-induced neuropathic pain. Mol. Pain 15, 1744806919840098 (2019). [PubMed: 30857460]
25. Flemming PK, Dedman AM, Xu SZ, Li J, Zeng F, Naylor J, Benham CD, Bateson AN, Muraki K, Beech DJ, Sensing of lysophospholipids by TRPC5 calcium channel. J. Biol. Chem 281, 4977–4982 (2006). [PubMed: 16368680]
26. Law S-H, Chan M-L, Marathe GK, Parveen F, Chen C-H, Ke L-Y, An updated review of lysophosphatidylcholine metabolism in human diseases. Int. J. Mol. Sci 20, 1149 (2019).
27. Burgos-Vega CC, Quigley LD, Trevisan dos Santos G, Yan F, Asiedu M, Jacobs B, Motina M, Safdar N, Yousuf H, Avona A, Price TJ, Dussor G, Non-invasive dural stimulation in mice: A novel preclinical model of migraine. Cephalalgia 39, 123–134 (2019). [PubMed: 29848109]
28. Burstein R, Yarnitsky D, Goor-Aryeh I, Ransil BJ, Bajwa ZH, An association between migraine and cutaneous allodynia. Ann. Neurol 47, 614–624 (2000). [PubMed: 10805332]
29. Ren C, Liu J, Zhou J, Liang H, Wang Y, Sun Y, Ma B, Yin Y, Lipidomic analysis of serum samples from migraine patients. Lipids Health Dis 17, 22 (2018). [PubMed: 29394939]
30. Song K, Wei M, Guo W, Kang Y, Wu J-X, Chen L, Structural basis for human TRPC5 channel inhibition by two distinct inhibitors. eLife 10, e63429 (2021). [PubMed: 33683200]
31. Just S, Chenard B, Cecl A, Strassmaier T, Chong J, Blair N, Gallaschun R, Camino D, Cantin S, D'Amours M, Eickmeier C, Fanger C, Hecker C, Hessler D, Hengerer B, Kroker K, Malekiani S, Mihalek R, McLaughlin J, Rast G, Witek J, Sauer A, Pryce C, Moran M, Treatment with HC-070, a potent inhibitor of TRPC4 and TRPC5, leads to anxiolytic and antidepressant effects in mice. PLOS ONE 13, e0191225 (2018). [PubMed: 29385160]

32. Miller M, Shi J, Zhu Y, Kustov M, Bin Tian J, Stevens A, Wu M, Xu J, Long S, Yang P, Zholos AV, Salovich JM, Weaver CD, Hopkins CR, Lindsley CW, McManus O, Li M, Zhu MX, Identification of ML204, a novel potent antagonist that selectively modulates native TRPC4/C5 ion channels. J. Biol. Chem 286, 33436–33446 (2011). [PubMed: 21795696]
33. Juarez-Salinas DL, Braz JM, Hamel KA, Basbaum AI, Pain relief by supraspinal gabapentin requires descending noradrenergic inhibitory controls. Pain Rep 3, e659 (2018). [PubMed: 30123855]
34. Wu H, Bogdanov M, Zhang Y, Sun K, Zhao S, Song A, Luo R, Parchim NF, Liu H, Huang A, Adebiyi MG, Jin J, Alexander DC, Milburn MV, Idowu M, Juneja HS, Kellems RE, Dowhan W, Xia Y, Hypoxia-mediated impaired erythrocyte Lands' Cycle is pathogenic for sickle cell disease. Sci. Rep 6, 29637 (2016). [PubMed: 27436223]
35. Mogil JS, Animal models of pain: Progress and challenges. Nat. Rev. Neurosci 10, 283–294 (2009). [PubMed: 19259101]
36. Shiers S, Klein RM, Price TJ, Quantitative differences in neuronal subpopulations between mouse and human dorsal root ganglia demonstrated with RNAscope in situ hybridization. Pain 161, 2410–2424 (2020). [PubMed: 32639368]
37. Murakami M, Taketomi Y, Secreted phospholipase A2 and mast cells. Allergol. Int 64, 4–10 (2015). [PubMed: 25572553]
38. Shepherd AJ, Mickle AD, Kadunganattil S, Hu H, Mohapatra DP, Parathyroid hormone-related peptide elicits peripheral TRPV1-dependent mechanical hypersensitivity. Front. Cell. Neurosci 12, 38 (2018). [PubMed: 29497363]
39. Wright DJ, Simmons KJ, Johnson RM, Beech DJ, Muench SP, Bon RS, Cryo-EM structures of human TRPC5 reveal interaction of a xanthine-based TRPC1/4/5 inhibitor with a conserved lipid binding site. bioRxiv 2020.04.17.047456 (2020).
40. Duan J, Li J, Chen G-L, Ge Y, Liu J, Xie K, Peng X, Zhou W, Zhong J, Zhang Y, Xu J, Xue C, Liang B, Zhu L, Liu W, Zhang C, Tian X-L, Wang J, Clapham DE, Zeng B, Li Z, Zhang J, Cryo-EM structure of TRPC5 at 2.8-Å resolution reveals unique and conserved structural elements essential for channel function. Sci. Adv 5, eaaw7935 (2019). [PubMed: 31355338]
41. Beech DJ, Bahnasi YM, Dedman AM, AL-Shawaf E, TRPC channel lipid specificity and mechanisms of lipid regulation. Cell Calcium 45, 583–588 (2009). [PubMed: 19324410]
42. Chaudhuri P, Colles SM, Bhat M, Van Wagoner DR, Birnbaumer L, Graham LM, Elucidation of a TRPC6-TRPC5 channel cascade that restricts endothelial cell movement. Mol. Biol. Cell 19, 3203–3211 (2008). [PubMed: 18495872]
43. Semtner M, Schaefer M, Pinkenburg O, Plant TD, Potentiation of TRPC5 by protons. J. Biol. Chem 282, 33868–33878 (2007). [PubMed: 17884814]
44. Beech DJ, Canonical transient receptor potential 5. Handb. Exp. Pharmacol 179, 109–123 (2007).
45. Gavva NR, Treanor JJS, Garami A, Fang L, Surapaneni S, Akrami A, Alvarez F, Bak A, Darling M, Gore A, Jang GR, Kesslak JP, Ni L, Norman MH, Palluconi G, Rose MJ, Salfi M, Tan E, Romanovsky AA, Banfield C, Davar G, Pharmacological blockade of the vanilloid receptor TRPV1 elicits marked hyperthermia in humans. Pain 136, 202–210 (2008). [PubMed: 18337008]
46. Mayorga AJ, Flores CM, Trudeau JJ, Moyer JA, Shalayda K, Dale M, Frustaci ME, Katz N, Manitpisitkul P, Treister R, Ratcliffe S, Romano G, A randomized study to evaluate the analgesic efficacy of a single dose of the TRPV1 antagonist mavatrep in patients with osteoarthritis. Scand. J. Pain 17, 134–143 (2017). [PubMed: 28850367]
47. Sevastou I, Kaffe E, Mouratis M-A, Aidinis V, Lysoglycerophospholipids in chronic inflammatory disorders: The PLA2/LPC and ATX/LPA axes. Biochim. Biophys. Acta Mol. Cell Biol. Lipids 1831, 42–60 (2013).
48. Zhang W, Sun G, Aitken D, Likhodii S, Liu M, Martin G, Furey A, Randell E, Rahman P, Jones G, Zhai G, Lysophosphatidylcholines to phosphatidylcholines ratio predicts advanced knee osteoarthritis. Rheumatol 55, 1566–1574 (2016).
49. Caboni P, Liori B, Kumar A, Santoru ML, Asthana S, Pieroni E, Fais A, Era B, Cacace E, Ruggiero V, Atzori L, Barton RH, Metabolomics analysis and modeling suggest a lysophosphocholines-PAF receptor interaction in fibromyalgia. PLOS ONE 9, e107626 (2014). [PubMed: 25238064]

50. Rabini RA, Galassi R, Fumelli P, Dousset N, Solera ML, Valdiguie P, Curatola G, Ferretti G, Taus M, Mazzanti L, Reduced Na^+-K+-ATPase activity and plasma lysophosphatidylcholine concentrations in diabetic patients. Diabetes 43, 915–919 (1994). [PubMed: 8013757]
51. Liu P, Duan J, Wang P, Qian D, Guo J, Shang E, Su S, Tang Y, Tang Z, Biomarkers of primary dysmenorrhea and herbal formula intervention: An exploratory metabonomics study of blood plasma and urine. Mol. Biosyst 9, 77–87 (2013). [PubMed: 23111557]
52. Hayakawa K, Kurano M, Ohya J, Oichi T, Kano K, Nishikawa M, Uranbileg B, Kuwajima K, Sumitani M, Tanaka S, Aoki J, Yatomi Y, Chikuda H, Lysophosphatidic acids and their substrate lysophospholipids in cerebrospinal fluid as objective biomarkers for evaluating the severity of lumbar spinal stenosis. Sci. Rep 9, 9144 (2019). [PubMed: 31235770]
53. Kuburas A, Mason BN, Hing B, Reis AS, Sowers LP, Moldovan Loomis C, Garcia-Martinez LF, Russo AF, PACAP induces light aversion in mice by an inheritable mechanism independent of CGRP. J. Neurosci, 10.1523/JNEUROSCI.2200-20.2021 (2021).
54. Kaiser EA, Russo AF, CGRP and migraine: Could PACAP play a role too? Neuropeptides 47, 451–461 (2013). [PubMed: 24210136]
55. Garcia RL, Schilling WP, Differential expression of mammalian TRP homologues across tissues and cell lines. Biochem. Biophys. Res. Commun 239, 279–283 (1997). [PubMed: 9345310]
56. Alawi KM, Russell FA, Aubdool AA, Srivastava S, Riffo-Vasquez Y, Baldissera L Jr., Thakore P, Saleque N, Fernandes ES, Walsh DA, Brain SD, Transient receptor potential canonical 5 (TRPC5) protects against pain and vascular inflammation in arthritis and joint inflammation. Ann. Rheum. Dis 76, 252–260 (2017). [PubMed: 27165180]
57. Beck B, Zholos A, Sydorenko V, Roudbaraki M, Lehen'kyi V, Bordat P, Prevarskaya N, Skryma R, TRPC7 is a receptor-operated DAG-activated channel in human keratinocytes. J. Invest. Dermatol 126, 1982–1993 (2006). [PubMed: 16741513]
58. Moehring F, Cowie AM, Menzel AD, Weyer AD, Grzybowski M, Arzua T, Geurts AM, Palygin O, Stucky CL, Keratinocytes mediate innocuous and noxious touch via ATP-P2X4 signaling. Elife 7, e31684 (2018). [PubMed: 29336303]
59. Baumbauer KM, DeBerry JJ, Adelman PC, Miller RH, Hachisuka J, Lee KH, Ross SE, Koerber HR, Davis BM, Albers KM, Keratinocytes can modulate and directly initiate nociceptive responses. Elife 4, e09674 (2015).
60. Riccio A, Li Y, Moon J, Kim KS, Smith KS, Rudolph U, Gapon S, Yao GL, Tsvetkov E, Rodig SJ, Van't Veer A, Meloni EG, Carlezon WA, Bolshakov VY, Clapham DE, Essential role for TRPC5 in amygdala function and fear-related behavior. Cell 137, 761–772 (2009). [PubMed: 19450521]
61. Kolber BJ, Montana MC, Carrasquillo Y, Xu J, Heinemann SF, Muglia LJ, Gereau RW IV, Activation of metabotropic glutamate receptor 5 in the amygdala modulates pain-like behavior 1/2 (ERK1/2). J. Neurosci 16, 8203–8213 (2010).
62. Crock LW, Kolber BJ, Morgan CD, Sadler KE, Vogt SK, Bruchas MR, Gereau RW IV, Central amygdala metabotropic glutamate receptor 5 in the modulation of visceral pain. J. Neurosci 32, 14217–14226 (2012). [PubMed: 23055491]
63. Phelan KD, Shwe UT, Abramowitz J, Wu H, Rhee SW, Howell MD, Gottschall PE, Freichel M, Flockerzi V, Birnbaumer L, Zheng F, Canonical transient receptor channel 5 (TRPC5) and TRPC1/4 contribute to seizure and excitotoxicity by distinct cellular mechanisms. Mol. Pharmacol 83, 429–438 (2013). [PubMed: 23188715]
64. Pászty C, Brion CM, Manci E, Witkowska HE, Stevens ME, Mohandas N, Rubin EM, Transgenic knockout mice with exclusively human sickle hemoglobin and sickle cell disease. Science 278, 876–878 (1997). [PubMed: 9346488]
65. Weyer AD, O'Hara CL, Stucky CL, Amplified mechanically gated currents in distinct subsets of myelinated sensory neurons following in vivo inflammation of skin and muscle. J. Neurosci 35, 9456–9462 (2015). [PubMed: 26109668]
66. Cowie AM, Stucky CL, A mouse model of postoperative pain. Bio-Protocol 9, e3140 (2019). [PubMed: 30820443]
67. Decosterd I, Woolf CJ, Spared nerve injury: An animal model of persistent peripheral neuropathic pain. Pain 87, 149–158 (2000). [PubMed: 10924808]

68. Sorge RE, Martin LJ, Isbester KA, Sotocinal SG, Rosen S, Tuttle AH, Wieskopf JS, Acland EL, Dokova A, Kadoura B, Leger P, Mapplebeck JCS, McPhail M, Delaney A, Wigerblad G, Schumann AP, Quinn T, Frasnelli J, Svensson CI, Sternberg WF, Mogil JS, Olfactory exposure to males, including men, causes stress and related analgesia in rodents. Nat. Methods 11, 629–632 (2014). [PubMed: 24776635]
69. Sadler KE, Zappia KJ, O'Hara CL, Langer SN, Weyer AD, Hillery CA, Stucky CL, Chemokine (C-C motif) receptor 2 mediates mechanical and cold hypersensitivity in sickle cell disease mice. Pain 159, 1652–1663 (2018). [PubMed: 29697532]
70. Chaplan SR, Bach FW, Pogrel JW, Chung JM, Yaksh TL, Quantitative assessment of tactile allodynia in the rat paw. J. Neurosci. Methods 53, 55–63 (1994). [PubMed: 7990513]
71. Dixon WJ, The up-and-down method for small samples. J. Am. Stat. Assoc 60, 967–978 (1965).
72. Hogan Q, Sapunar D, Modric-Jednacak K, McCallum JB, Detection of neuropathic pain in a rat model of peripheral nerve injury. Anesthesiology 101, 476–487 (2004). [PubMed: 15277932]
73. Cowie AM, Moehring F, O'Hara C, Stucky CL, Optogenetic inhibition of CGRPa sensory neurons reveals their distinct roles in neuropathic and incisional pain. J. Neurosci 38, 5807–5825 (2018). [PubMed: 29925650]
74. King T, Vera-Portocarrero L, Gutierrez T, Vanderah TW, Dussor G, Lai J, Fields HL, Porreca F, Unmasking the tonic-aversive state in neuropathic pain. Nat. Neurosci 12, 1364–1366 (2009). [PubMed: 19783992]
75. Griggs RB, Bardo MT, Taylor BK, Gabapentin alleviates affective pain after traumatic nerve injury. Neuroreport 26, 522–527 (2015). [PubMed: 26011387]
76. Cunningham CL, Ferree NK, Howard MA, Apparatus bias and place conditioning with ethanol in mice. Psychopharmacology 170, 409–422 (2003). [PubMed: 12955296]
77. Reeh PW, Sensory in vitro preparation. Prog. Brain Res 74, 271–276 (1988). [PubMed: 3187037]
78. Koltzenburg M, Stucky CL, Lewin GR, Receptive properties of mouse sensory neurons innervating hairy skin. J. Neurophysiol 78, 1841–1850 (1997). [PubMed: 9325353]
79. Sostare J, Di Guida R, Kirwan J, Chalal K, Palmer E, Dunn WB, Viant MR, Comparison of modified Matyash method to conventional solvent systems for polar metabolite and lipid extractions. Anal. Chim. Acta 1037, 301–315 (2018). [PubMed: 30292307]
80. Akbulut Y, Gaunt HJ, Muraki K, Ludlow MJ, Amer MS, Bruns A, Vasudev NS, Radtke L, Willot M, Hahn S, Seitz T, Ziegler S, Christmann M, Beech DJ, Waldmann H, Englerin a is a potent and selective activator of TRPC4 and TRPC5 calcium channels. Angew. Chem. Int. Ed 54, 3787–3791 (2015).
81. Rostock C, Schrenk-Siemens K, Pohle J, Siemens J, Human vs. mouse nociceptors – Similarities and differences. Neuroscience 387, 13–27 (2018). [PubMed: 29229553]

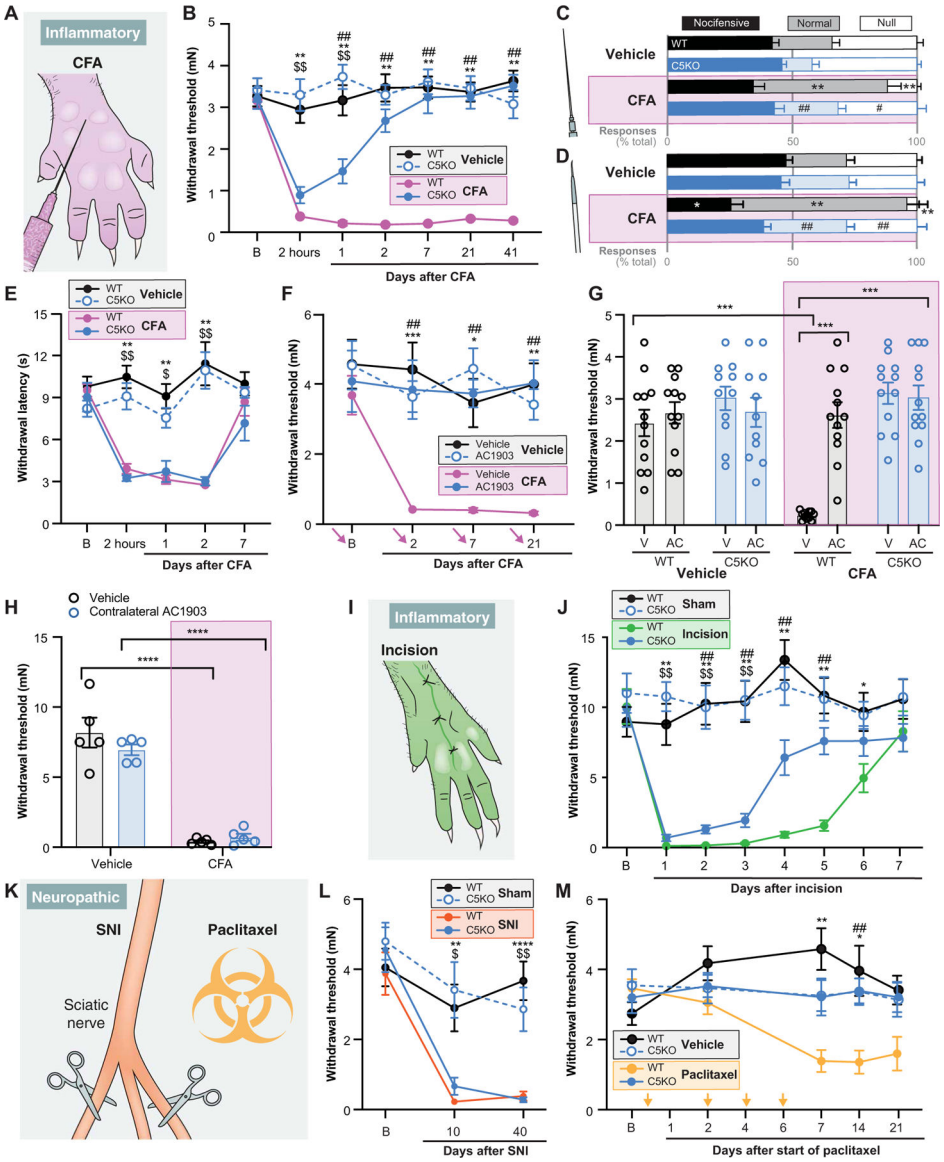

Fig. 1. TRPC5 contributes to persistent mechanical hypersensitivity in inducible inflammatory pain models.

(**A**) Depiction of complete Freund's adjuvant (CFA) model. (**B**) Mechanical withdrawal thresholds of global TRPC5 knockout (C5KO) and wild-type (WT) mice after CFA injection; $n = 11$ to 12. (**C**) Response characterization to noxious needle hindpaw stimulation 9 days after CFA; $n = 6$ to 10. (**D**) Response characterization to paintbrush swiping across plantar hindpaw 9 days after CFA; $n = 6$ to 10. (**E**) Withdrawal latencies to radiant heat stimulus; $n = 10$. (**F**) Mechanical withdrawal thresholds 60 min after intraplantar injection of AC1903; $n = 10$; arrows indicate injection on each day. (**G**) Mechanical withdrawal thresholds on day 41 after CFA, 60 min after intraplantar injection of AC1903 (AC) or vehicle (V); $n = 11$ to 12; Bonferroni post hoc comparison, $^{***}P < 0.001$. (**H**) Mechanical withdrawal thresholds of CFA-injected paw 60 min after intraplantar injection of AC1903 in contralateral paw; $n = 5$; Bonferroni post hoc comparison, $^{****}P < 0.0001$. (**I**) Depiction of plantar incision model. (**J**) Mechanical withdrawal thresholds after hindpaw

plantar incision; $n = 17$ to 21. (**K**) Depiction of spared nerve injury (SNI) and paclitaxel neuropathic pain models. (**L**) Mechanical withdrawal thresholds after SNI; $n = 7$ to 10. (**M**) Mechanical withdrawal thresholds after paclitaxel; $n = 8$ to 10; arrows indicate paclitaxel injections. Three-way analysis of variance (ANOVA) performed on (B), (E) to (G), (J), (L), and (M); chi-square performed on (C) and (D); two-way ANOVA performed on (H). Post hoc comparisons (Bonferroni or Fisher's exact) for all panels unless otherwise stated, *$P <$ 0.05, **$P < 0.01$, and ***$P < 0.001$ wild-type control versus injury; \$$P < 0.05$ and \$ \$$P <$ 0.01 C5KO control versus injury; #$P < 0.05$ and ##$P < 0.01$ injury C5KO versus wild-type. All data are means ± SEM; B, baseline; AC1903 dose, 50 μg.

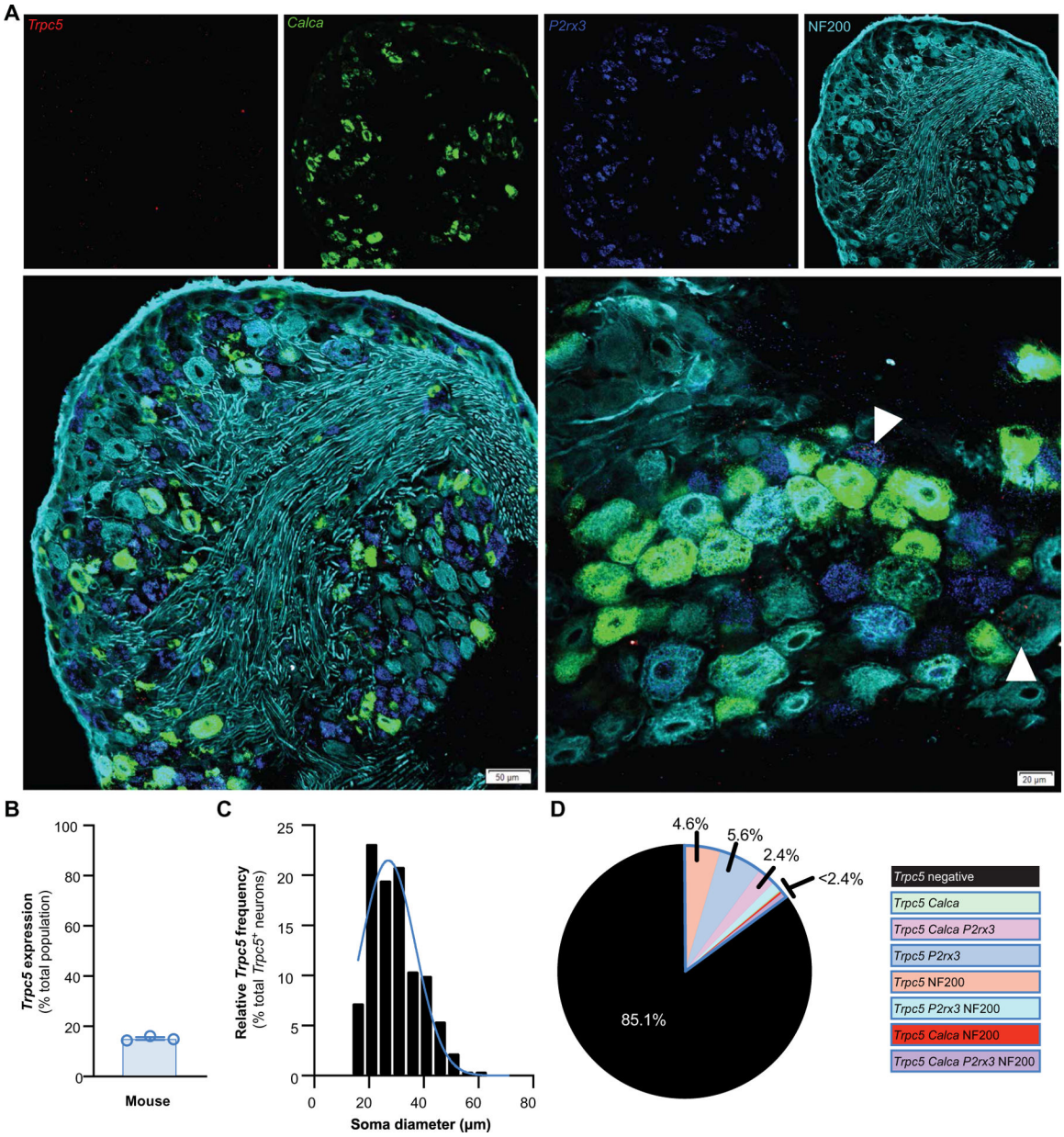

Fig. 2. Mouse *Trpc5* is expressed in peripheral sensory neurons.

(**A**) Representative 20× and 40× images of mouse DRG after RNAscope in situ hybridization for *Trpc5* (red), CGRP (*Calca*; green), P2X3R (*P2rx3*; blue), and NF200 (neurofilament 200; cyan); scale bar, 50 μm (20×) and 20 μm (40×). Arrowheads in 40× image highlight *P2rx3*-positive neuron and NF200-positive neuron that express *Trpc5*. (**B**) Percentage of DRG neurons that express *Trpc5*; $n = 3$ mice. (**C**) Size distribution of *Trpc5*-positive neurons; $n = 1476$ neurons from three mice; bars are averages. (**D**) Coexpression characterization of *Trpc5*-positive neurons; pie wedges are averages; $n = 1476$ neurons from three mice.

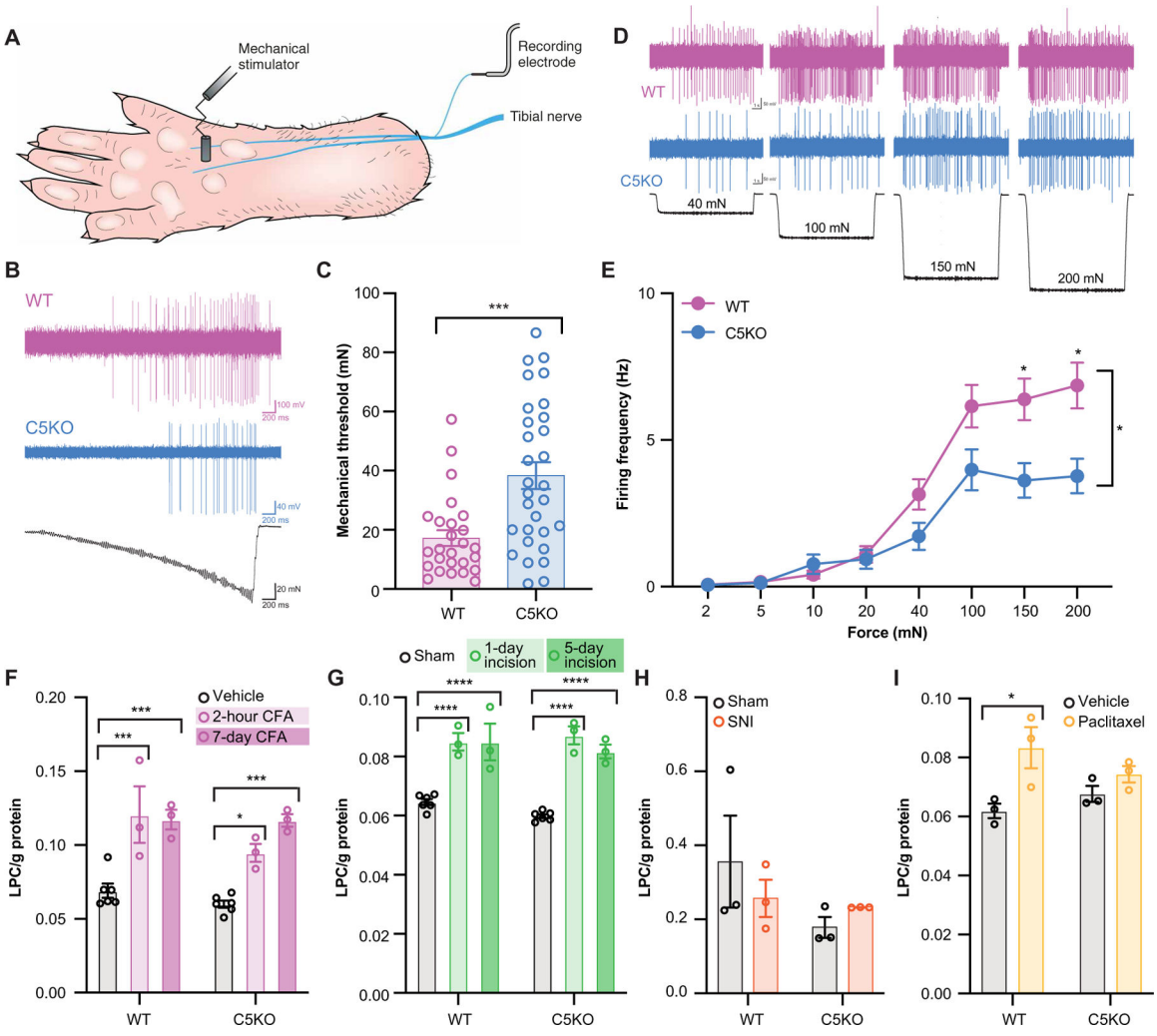

Fig. 3. Peripherally expressed TRPC5 mediates mechanical hypersensitivity after injuries associated with elevated concentrations of LPC.

(**A**) Schematic of teased fiber recordings. (**B**) Representative C fiber activity traces during force ramp application (10 s; up to 100 mN). Force ramps were used to determine the mechanical threshold of each fiber. (**C**) Mechanical thresholds of fibers from CFA-injected wild-type and C5KO mice; $n = 27$ to 30 units from five mice; Mann-Whitney test, ***$P < 0.001$. (**D**) Representative C fiber activity during static force application. (**E**) Mean mechanically induced firing rates of C fibers from CFA-injected mice; $n = 27$ to 30 units from five mice, two-way ANOVA effect of genotype, *$P < 0.05$. (**F**) Amount of LPC in skin 2 hours and 7 days after CFA injection; $n = 3$ to 6. (**G**) Amount of LPC in skin 1 and 5 days after hindpaw plantar incision; $n = 3$ to 6. (**H**) Amount of LPC in sciatic nerve 10 days after SNI; $n = 3$. (**I**) Amount of LPC in skin 21 days after first paclitaxel injection; $n = 3$. Two-way ANOVA performed on (F) to (I). Bonferroni post hoc comparisons for all panels, *$P < 0.05$, ***$P < 0.001$, and ****$P < 0.0001$. All data are means ± SEM.

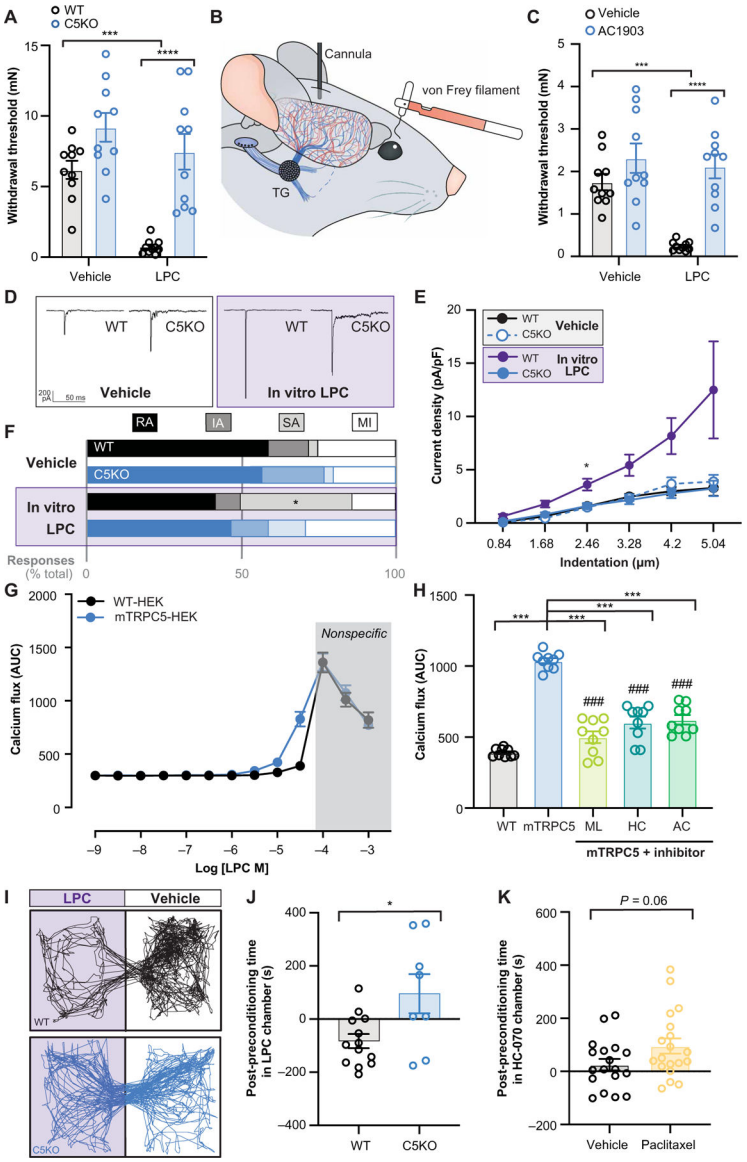

Fig. 4. LPC induces behavioral and neuronal mechanical hypersensitivity in TRPC5-dependent fashion.

(**A**) Mechanical withdrawal thresholds of C5KO or wild-type mice 45 to 60 min after intraplantar injection of 50 μM LPC; $n = 10$. (**B**) Schematic of dural injection and facial von Frey testing. (**C**) Periorbital mechanical withdrawal thresholds 60 min after dural application of 4.8 nM LPC and/or 50 μg of AC1903; $n = 10$. (**D**) Representative current traces from trigeminal ganglia (TG) neurons during mechanical stimulation. (**E**) Mean mechanical current density of TG neurons during 250 nM LPC incubation; $n = 24$ to 30 neurons from three to five mice. (**F**) Characterization of TG mechanical currents as rapidly adapting (RA), intermediate adapting (IA), slowly adapting (SA), or mechanically insensitive (MI); $n = 30$ to 36 neurons from >3 mice. (**G**) LPC-mediated calcium flux in HEK cells untransfected or stably expressing mTRPC5; $n = 3$ independent replicates performed in triplicate. (**H**) Quantification of LPC (32 μM)–induced calcium flux in HEK cells untransfected or stably expressing mTRPC5 and incubated with ML204 (320 μM), HC-070 (100 μM), or AC1903

(320 μM); $n = 3$ or more independent replicates performed in triplicate; Bonferroni post hoc, ###$P < 0.001$ wild-type versus inhibitor. (**I**) Representative track plots of wild-type and C5KO mice in two-chamber box during postconditioning test; subcutaneous LPC injection (5 μM) associated with purple box, vehicle injection associated with white box. (**J**) Difference in LPC chamber time between pre- and postconditioning trials; $n = 8$ to 13; unpaired t test, *$P < 0.05$. (**K**) Difference in HC-070 chamber time between pre- and postconditioning trials; $n = 18$ to 20; unpaired t test, $P = 0.06$. Two-way ANOVA performed on (A), (C), and (G); chi-square performed on (F); three-way ANOVA performed on (E); one-way ANOVA performed on (H). Bonferroni post hoc comparisons for all panels, *$P <$ 0.05, ***$P < 0.001$, and ****$P < 0.0001$. All data are means ± SEM.

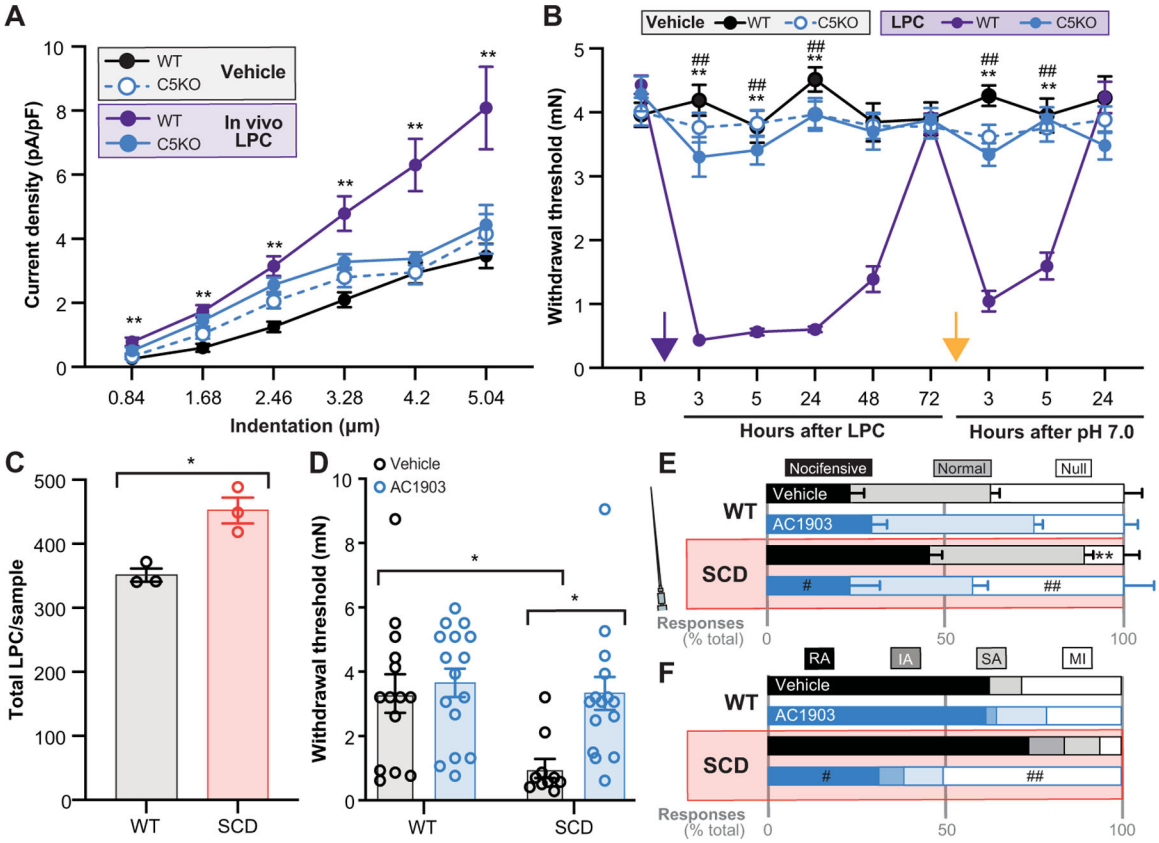

Fig. 5. After initial exposure to LPC, TRPC5 activity mediates mechanical hypersensitivity even in the absence of LPC.

(**A**) Mean mechanical current density of TG neurons isolated from mice 24 hours after dural application of 4.8 nM LPC; $n = 33$ to 45 cells from three to five mice; three-way ANOVA, followed by Bonferroni post hoc comparison, $^{**}P < 0.01$ wild-type vehicle versus LPC. (**B**) Periorbital mechanical withdrawal thresholds after dural application of 1.2 nM LPC and pH 7.0 PBS; $n = 10$ to 15; purple arrow indicates LPC injection, yellow arrow indicates pH 7.0 PBS injection; three-way ANOVA, followed by Bonferroni post hoc comparison, $^{**}P < 0.01$ wild-type vehicle versus LPC and $\#\#\ P < 0.01$ LPC wild-type versus C5KO. (**C**) Relative amount of LPC in serum of wild-type and sickle cell disease (SCD) mice; $n = 3$, unpaired t test $^{*}P < 0.05$. (**D**) Mechanical withdrawal thresholds 60 min after intraplantar injection of AC1903 (50 μg); $n = 10$ to 14; two-way ANOVA, followed by Bonferroni post hoc comparisons, $^{*}P < 0.05$. (**E**) Response characterization to noxious needle hindpaw stimulation 60 min after intraplantar injection of AC1903 (50 μg); $n = 9$ to 10; chi-square, followed by Fisher's exact test, $^{**}P < 0.01$ vehicle wild-type versus SCD, $\#P < 0.05$, and $\#\#P < 0.01$ SCD vehicle versus AC1903. (**F**) Characterization of DRG mechanical currents as RA, IA, SA, or MI; chi-square, followed by Fisher's exact test, $\#P < 0.05$ and $\#\#P < 0.01$ SCD vehicle versus AC1903; $n = 28$ to 32 neurons from three to five mice. All data are means ± SEM unless otherwise stated.

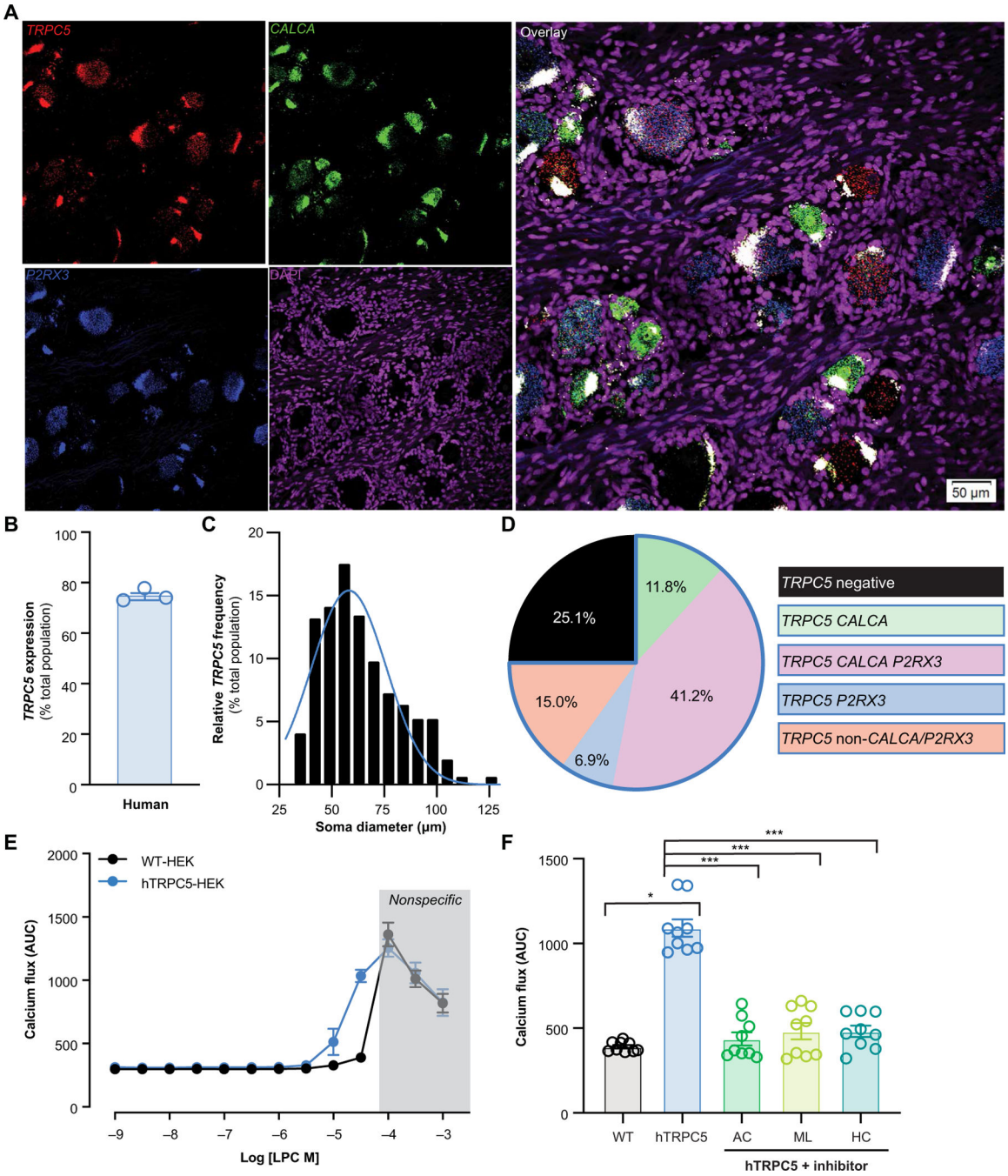

Fig. 6. hTRPC5 is expressed by most of the DRG neurons and activated by LPC.

(**A**) Representative 20× image of human DRG neurons after RNAscope in situ hybridization for TRPC5 (red), CGRP (*CALCA*; green), P2XR3 (*P2RX3*; blue), and DAPI (magenta); scale bar, 50 µM. (**B**) Percentage of DRG neurons that express TRPC5; $n = 3$ humans. (C) Frequency of TRPC5-positive neurons across population of human DRG neurons; $n =$ 438 neurons from three humans; bars are averages. (**D**) Coexpression characterization of TRPC5-positive and TRPC5-negative neurons; pie wedges are averages; $n = 580$ neurons from three humans. (**E**) LPC-mediated calcium flux in HEK cells untransfected or stably

expressing hTRPC5; $n = 3$ independent replicates performed in triplicate. (**F**) Quantification of LPC (32 μM)–induced calcium flux in HEK cells untransfected or stably expressing hTRPC5 and incubated with ML204 (320 μM), HC-070 (100 μM), or AC 1903 (320 μM); $n = 3$ independent replicates performed in triplicate; two-way ANOVA performed on (E), one-way ANOVA performed on (F), Bonferroni post hoc comparisons, $*P < 0.05$ and $***P < 0.001$. All data are means ± SEM unless otherwise stated.

Table 1.

Relative amount of LPC species in skin 2 hours and 7 days after CFA, 1 and 5 days after hindpaw plantar incision, or 21 days after first paclitaxel injection.

	CFA						Incision						Paclitaxel		
	2 Hours			7 Days			1 Day			5 Days					
	WT CFA	**C5KO vehicle**	**C5KO CFA**	**WT CFA**	**C5KO vehicle**	**C5KO CFA**	**WT incision**	**C5KO sham**	**C5KO incision**	**WT incision**	**C5KO sham**	**C5KO incision**	**WT paclitaxel**	**C5KO vehicle**	**C5KO paclitaxel**
(15:0)	0.98	0.94	1.12	*1.68*	0.76	**1.53** **	1.18	0.97	*1.35* **	*1.81*	0.44	1.63	1.19	1.08	1.05
(16:0)	**1.55**	0.84	**1.67** ***	2.03	0.99	2.21 ***	**1.35** ***	0.81	**1.35** ***	*1.52*	1.07	1.49	*1.24*	1.04	1.13
(16:1)	1.34	1.07	1.49	1.73	0.95	1.73	*1.38* *	1.05	*1.39* *	1.35	0.96	1.19	1.26	1.25	1.04
(17:0)	1.29	1.00	1.54	*1.52*	0.88	*1.53* *	1.23*	0.90	1.19	1.02	0.89	1.12	0.98	1.03	1.08
(18:0)	*2.00*	0.74	1.51	1.38	0.89	1.45 ***	**1.30** ***	*0.73*	**1.30** ***	*1.15*	0.81	1.09*	*1.29*	1.03	1.14
(18:1)	*1.87* *	1.01	**2.17** **	**2.04**	0.98	*2.06* *	1.49 ***	0.97	**1.43** ***	1.39	0.93	1.30	1.33	1.18	1.17
(18:2)	1.89	1.32	*2.23*	1.81	0.90	1.78	2.25 **	1.45	*1.67*	1.25	1.04	**1.24** **	1.11	0.92	0.88
(18:3)	nd	nd	nd	1.81	1.02	1.73	X	X	nd	1.39	0.98	1.65	nd	nd	nd
(20:0)	1.26	1.05	**1.64** **	nd	nd	X	*1.44*	1.14	1.16	2.17	nd	5.53	1.03	1.01	0.92
(20:1)	1.72	1.29	**2.37** *	1.31	0.80	1.14	2.05 ***	1.19	*1.39*	1.16	0.87	0.95	1.06	1.04	0.86
(20:2)	1.90	1.15	1.83	*X*	nd	**X** *	**1.79**	1.33	1.51	X	X	X	0.89	0.80	0.81
(20:3)	2.53 ***	1.04	2.91 ***	**1.94**	1.06	*2.32*	1.86 **	1.35	*1.44*	1.36	0.84	1.71	1.37	1.01	1.03
(20:4)	1.83 ***	0.83	1.93 ***	*2.14*	1.13	1.82*	1.82 ***	1.09	1.81 ***	1.26	1.09	1.17	1.40	1.00	1.07
(22:0)	1.04	0.89	1.20	1.88	0.97	1.85	0.96	0.95	0.94	1.40	0.77	1.23	1.01	1.01	0.92
(22:4)	3.20	nd	2.25	nd	nd	nd	1.23	0.79	nd	nd	nd	nd	X	X	nd
(22:5)	X	nd	X	0.97	1.03	nd	nd	nd	nd	0.87	1.16	nd	nd	nd	nd
(22:6)	4.57*	nd	**5.83** **	X	nd	nd	**X**	X	*X*	nd	nd	nd	1.44	1.07	nd

Values are fold increases relative to wild-type (WT) sham/vehicle. Italic text, $P < 0.05$ versus wild-type sham; bold text, $P < 0.01$ versus wild-type sham; underlined text, $P < 0.001$ versus wild-type sham;

* $P < 0.05$ versus C5KO sham;

** $P < 0.01$ versus C5KO sham;

***$P < 0.001$ versus C5KO sham; nd, not detected in any sample; X, not detected in wild-type sham; $n = 3$ mice.

Table 2.

Relative amount of serum LPC species in Berk SS sickle cell disease (SCD) mice, wild-type and C5KO mice 7 days after CFA, 5 days after hindpaw plantar incision, 10 days after SNI, or 21 days after first paclitaxel injection.

		CFA			Incision			SNI			Paclitaxel		
	SCD	WT CFA	C5KO vehicle	C5KO CFA	WT incision	C5KO sham	C5KO incision	WT SNI	C5KO sham	C5KO SNI	WT paclitaxel	C5KO vehicle	C5KO paclitaxel
(15:0)	0.95	0.38	1.74	0.86	0.93	0.76	0.94	0.83	0.89	0.99	0.66	0.64	0.59
(16:0)	*1.15*	0.86	1.20	0.95	0.94	0.97	1.05	1.10	0.83	1.01	0.87	0.87	0.91
(16:1)	**2.17**	0.87	1.08	0.93	**0.68**	0.92	0.86	1.12	0.88	0.94	1.22	1.18	1.55
(17:0)	0.87	0.77	1.31	0.93	0.89	0.85	1.09	1.13	1.07	1.24	0.81	0.84	0.77
(18:0)	0.96	0.95	1.23	1.10	0.91	0.96	1.17	1.14	0.78	0.97	0.85	0.87	0.81
(18:1)	**2.12**	0.89	1.04	0.94	0.79	0.96	0.77	1.09	0.90	0.85	1.26	1.43	1.46
(18:2)	*1.39*	0.95	1.17	0.97	0.84	0.83	1.01	1.00	0.95	0.85	0.92	1.02	1.22
(18:3)	2.08	0.58	0.81	0.70	nd	1.13	0.92	nd	1.18	nd	0.92	0.96	2.07
(20:0)	**0.39**	1.23	1.29	0.98	1.09	1.17	1.08	1.32	1.44	*3.12*	**0.31**	**0.29**	**0.37**
(20:1)	0.90	0.80	1.09	0.88	1.04	1.24	0.99	1.49	1.14	1.63	0.71	*0.60*	*0.59*
(20:2)	**1.79**	0.95	0.95	1.06	0.88	0.94	*0.72*	1.13	0.97	1.25	1.00	0.96	1.00
(20:3)	**1.77**	1.08	1.03	1.06	0.84	1.00	0.77	1.08	0.96	0.97	1.07	1.13	1.16
(20:4)	**2.83**	0.82	1.20	0.78	0.82	0.69	1.05 *	0.94	0.71	0.62	1.19	1.08	1.53
(20:5)	nd	nd	nd	X	nd	nd	nd	nd	nd	nd	X	X	X
(22:4)	**7.34**	0.75	0.59	0.89	1.13	0.96	0.84	1.10	0.82	1.05	0.26	0.70	0.57
(22:5)	*1.81*	0.81	0.85	0.84	*0.68*	**0.59**	**0.54**	1.19	0.62	1.04	*0.55*	*0.54*	0.68
(22:6)	**2.05**	0.83	1.33	0.96	0.85	1.06	*1.34*	1.17	1.15	0.94	1.00	0.95	1.29

Values are fold increases relative to wild-type (WT) sham/vehicle. Italic text, $P < 0.05$ versus wild-type sham; bold text, $P < 0.01$ versus wild-type sham;

* $P < 0.05$ versus C5KO sham; nd, not detected in any sample; X, not detected in wild-type sham; $n = 3$ mice.